Period-doubling route to mixed-mode chaos

Naziru M. Awal and Irving R. Epstein*
Department of Chemistry, Brandeis University, Waltham, Massachusetts 02453, USA

(Received 1 October 2020; revised 15 July 2021; accepted 16 July 2021; published 12 August 2021)

Mixed-mode oscillations (MMOs) are a complex dynamical behavior in which each cycle of oscillation consists of one or more large amplitude spikes followed by one or more small amplitude peaks. MMOs typically undergo period-adding bifurcations under parameter variation. We demonstrate here, in a set of three identical, linearly coupled van der Pol oscillators, a scenario in which MMOs exhibit a period-doubling sequence to chaos that preserves the MMO structure, as well as period-adding bifurcations. We characterize the chaotic nature of the MMOs and attribute their existence to a master-slave-like forcing of the inner oscillator by the outer two with a sufficient phase difference between them. Simulations of a single nonautonomous oscillator forced by two sine functions support this interpretation and suggest that the MMO period-doubling scenario may be more general.

DOI: 10.1103/PhysRevE.104.024211

I. INTRODUCTION

Period-doubling (PD) and mixed-mode oscillations (MMOs) are two of the major paradigms of nonlinear dynamics. In PD, as a parameter is varied, alternate, previously equal extrema of a periodic orbit assume different values, thereby doubling the period of the oscillation and ultimately leading to chaos. MMOs are periodic oscillations consisting of M large (LAOs) and n small (SAOs) amplitude oscillations per cycle (M^n). On varying a parameter, MMOs typically undergo period-adding bifurcations, e.g., from M^n to M^{n+1} [1–4]. In this work, we describe a bifurcation sequence, in which a single type of MMO exhibits PD bifurcations leading to chaos in its SAOs only, while its LAOs and its M^n structure remain unchanged.

Mixed-mode oscillations have been studied in many systems. For example chemical systems such as the Belousov-Zhabotinsky reaction have been reported to show MMOs [1,5–10]. MMOs are also found in neural systems [11–19] as well as in electrochemical systems [20–24]. Some of these systems exhibit complex MMOs under weak perturbations. Over long time intervals, the MMOs occasionally produce bursts, thereby making the system chaotic, in what the authors sometimes refer to as intermittent chaotic MMOs. In such cases, both the LAOs and SAOs behave chaotically [25]. Studies performed in developing inner hair cells have revealed that complex MMO oscillations can be produced [26,27]. The period doubling to chaos is observed with additional periods added to the small amplitude oscillations until the system shows mixed patterns as shown in label 4 of Fig. 3 b in Ref. [26]. The work we present here is different because the period doubling occurs with the whole MMOs but it is apparent only by looking at the small amplitude oscillations. The MMOs structure is maintained as the system goes to chaos.

We analyze here a system of three van der Pol oscillators [28,29] in Liénard form coupled linearly [see Fig. 1(a)] through diffusion of the variable, w, which is analogous to the recovery variable in the FitzHugh-Nagumo model [30,31]. The system evolves as shown in Eq. (1). With this model, there is no direct link between the outer oscillators 1 and 3, though they interact indirectly through the central oscillator 2. The system is invariant to exchange of oscillators 1 and 3,

$$\begin{aligned}
\frac{dv_1}{dt} &= -hv_1^3 + av_1 - w_1,\\
\frac{dw_1}{dt} &= \varepsilon(v_1 - \varphi) + D_w(w_2 - w_1),\\
\frac{dv_2}{dt} &= -hv_2^3 + av_2 - w_2,\\
\frac{dw_2}{dt} &= \varepsilon(v_2 - \varphi) + D_w(w_3 - 2w_2 + w_1),\\
\frac{dv_3}{dt} &= -hv_3^3 + av_3 - w_3,\\
\frac{dw_3}{dt} &= \varepsilon(v_3 - \varphi) + D_w(w_2 - w_3),
\end{aligned} \tag{1}$$

where $0 < \varepsilon \ll 1$, h, and a are nonnegative constants, φ determines the relative position of the w nullcline with respect to the v nullcline for an uncoupled system and D_w represents the coupling strength.

II. RESULTS

A. Fully coupled system

Numerical simulations of Eq. (1) show a variety of interesting dynamics, keeping h, a, ε and D_w constant, as we vary φ. The dynamics of system (1) depends on the value of φ, i.e., on the relative position of the w nullcline with respect to the v nullcline. The orbit diagram in Fig. 2(a) shows four regions where different behaviors are observed. In Region I, at low φ, the three oscillators display

*epstein@brandeis.edu

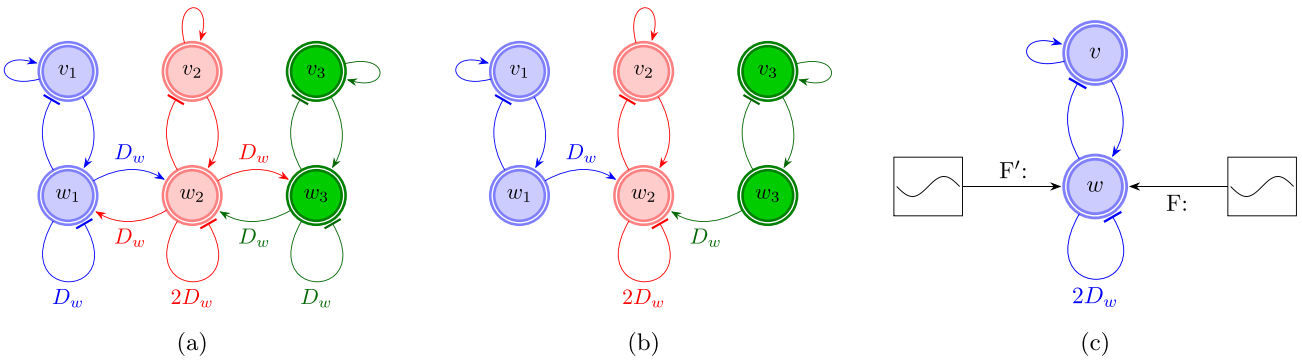

FIG. 1. Representation of different coupling schemes. (a) Fully coupled. (b) Master-slave. (c) Forced uncoupled.

a homogeneous steady state followed by nearly harmonic in-phase SAOs born through a supercritical Hopf bifurcation as φ increases. By increasing φ further (Region II), a transition to in-phase LAOs for two of the oscillators may occur via a canard explosion, where an oscillator switches from SAOs to LAOs with an infinitesimal change in the bifurcation parameter, while one of the oscillators maintains its SAOs. As φ increases, all oscillators transition to in-phase LAOs before breaking symmetry, allowing one of the oscillators to display SAOs. The oscillator with the SAOs goes through triperiodic oscillations followed by quasiperiodic oscillations and then chaos. We observe two symmetry breakings (SB), one involving oscillator 3 and the other with oscillator 2 [Region II of Fig. 2(a)]. For different initial conditions, either one oscillator undergoes a reverse canard or no symmetry-breaking occurs. The symmetry breaking shown in

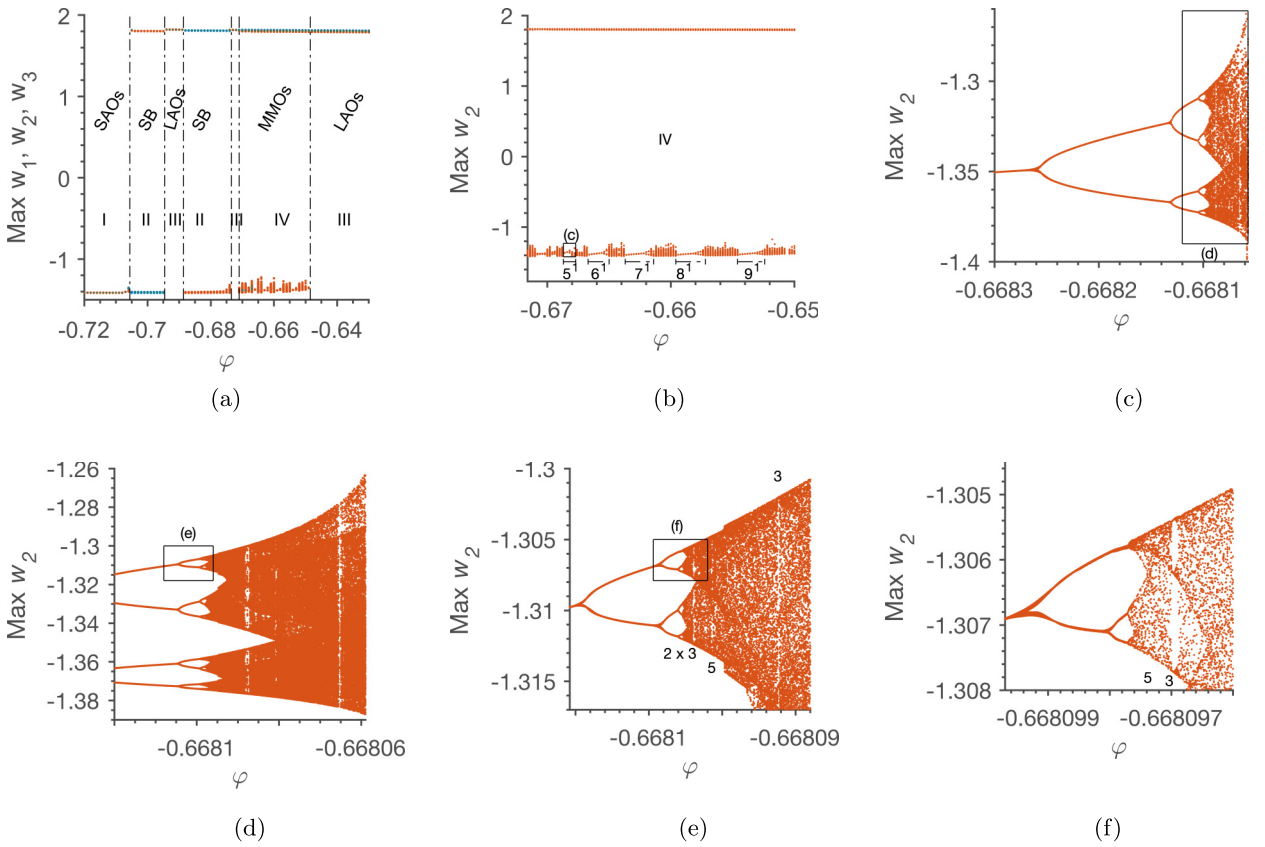

FIG. 2. Orbit diagram showing maximum amplitude of oscillations with varying φ. Parameters: $a = 3.0$, $\varepsilon = 0.1335$, $h = 2.0$ and $D_w = 1.865 \times 10^{-3}$. Initial conditions: $(v_1,\ w_1) = (-0.6242,\ -1.31378)$, $(v_2,\ w_2) = (0.15636,\ 1.79106)$, and $(v_3,\ w_3) = (0.97553,\ 1.14483)$. (a) All three oscillators. (b) Oscillator 2. (c) Expanded from Fig. 2(b). (d) Expanded from Fig. 2(c). (e) Expanded from Fig. 2(d). (f) Expanded from Fig. 2(e). Blue: oscillator 1, red: oscillator 2, green: oscillator 3. In (a), where blue, red, and green overlap, only green is seen. Similarly, only green is seen where blue and green overlap. Black boxes labeled with letters indicate region expanded in the following panel.

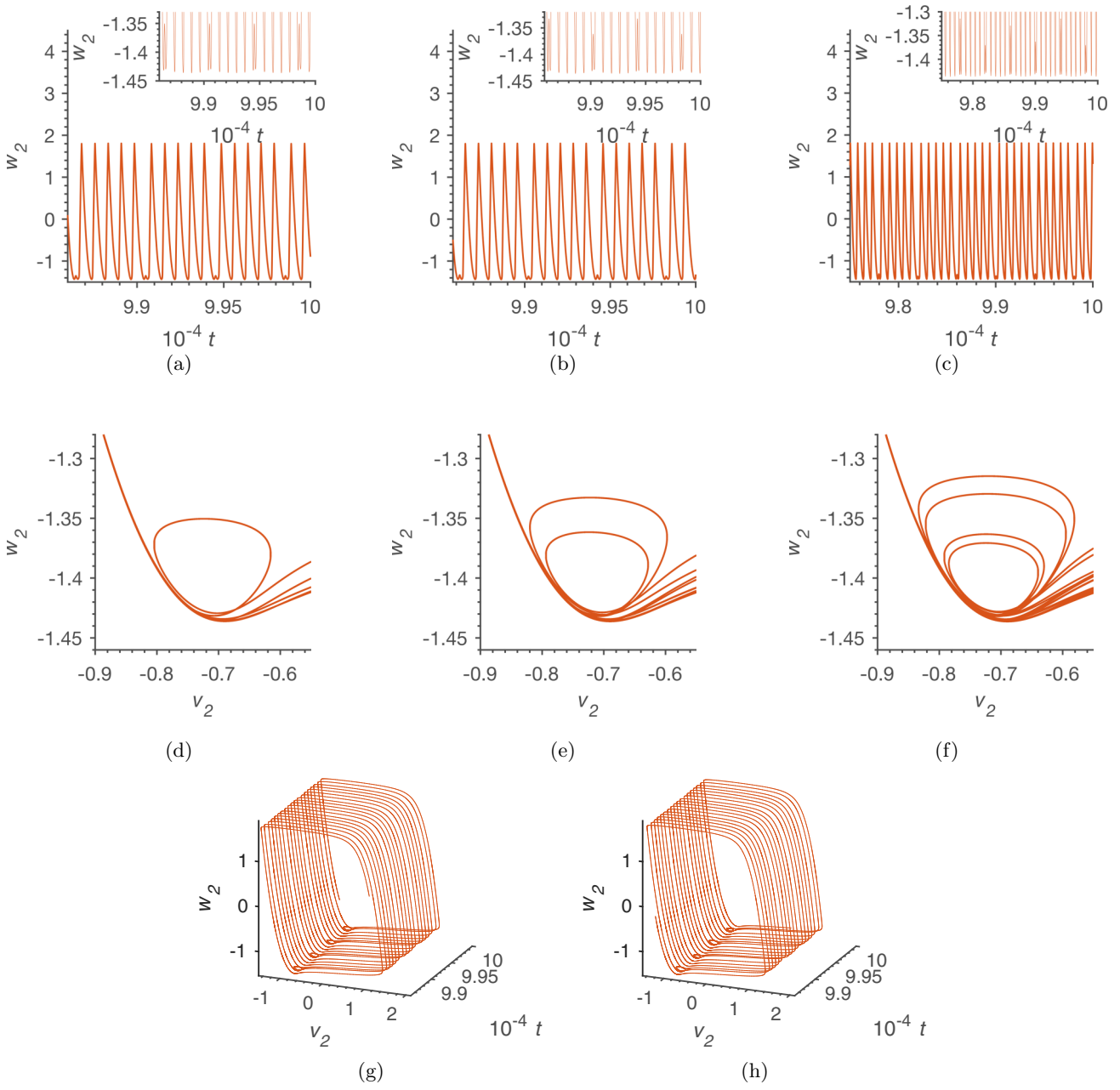

FIG. 3. Time series and phase portraits of oscillator 2 from numerical simulations. Parameters and initial conditions: same as Fig. 2. Top: time series; middle panel: phase portraits; bottom panel: 3D plot of v_2, w_2 vs. time. (a), (d), (g) Period-6 MMOs at $\varphi = -0.66830$. (b), (e), (h) Period-12 MMOs at $\varphi = -0.66820$. (c), (f) Period-24 MMOs at $\varphi = -0.66812$.

Regions II of Fig. 2(a), in which identical coupled oscillators display chimeralike behavior, with one showing nearly periodic LAOs and the other aperiodic SAOs, resembles that seen in earlier work [32,33] on coupled Lengyel-Epstein oscillators and with heterogeneous phase oscillators [34–36] where the coupling strength, phase lags and other parameters used in the studies were different and with nonlocal coupling. In Regions III, all three oscillators exhibit in-phase LAOs, oscillating with the same amplitude, period, and phase.

Our focus in this work is on Region IV, which extends from $\varphi \approx -0.66830$ to $\varphi \approx -0.648264$. In this region, oscillator 2 begins to exhibit MMOs. We observe five distinct MMO patterns, each of which displays a period-doubling sequence to chaos as φ increases, as shown in Fig. 2(b). After each MMO pattern, a brief period of chaotic mixed-pattern MMOs is observed before the system transitions to the next pattern. For instance, after the period doubling to chaos in the 5^1 MMOs, we observe a mixture of 5^1 and 6^1 MMOs before the 6^1 MMO region begins [similar to the mixture of 6^1 and 7^1 MMOs in Fig. 4(b)]. We focus here on the M^1 MMOs, especially the 5^1 patterns observed in Fig. 2(b). The small maximum corresponds to nearly harmonic SAOs that occur near the minimum of the cubic nullcline, while the large maxima correspond to relaxation-type LAOs.

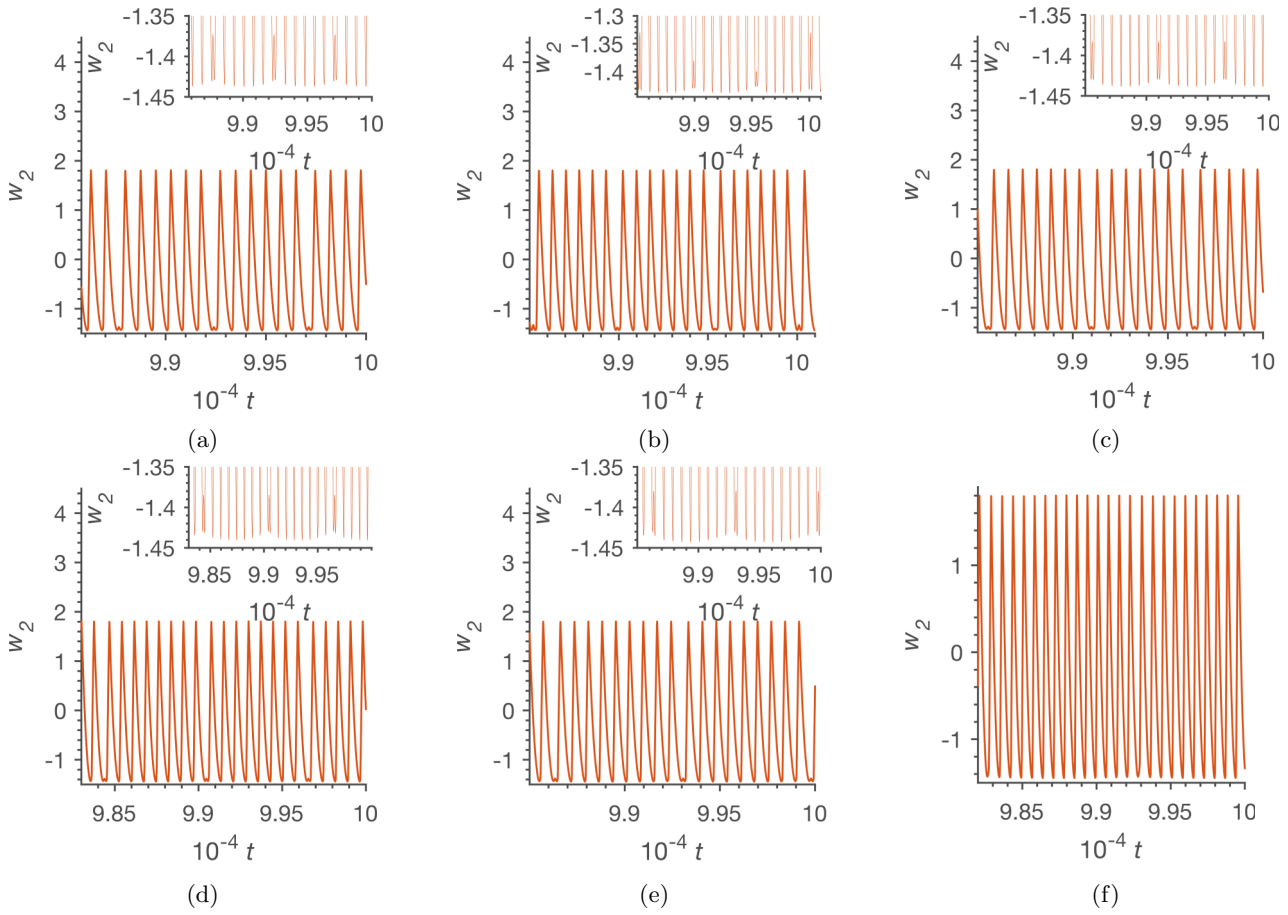

FIG. 4. Time series of oscillator 2 obtained from numerical simulations. Parameters and initial conditions: same as Fig. 2. (a) 6^1 period-1 (Period-7) MMOs at $\varphi = -0.6659$. (b) Combination of 6^1 and 7^1 MMOs at $\varphi = -0.66455$. (c) 7^1 MMOs at $\varphi = -0.6630$. (d) 8^1 MMOs at $\varphi = -0.6590$. (e) 9^1 MMOs at $\varphi = -0.6540$. (f) 1^0 oscillations at $\varphi = -0.648264$.

Figure 2(b) shows the orbit diagram for oscillator 2 for $-0.6688 \leqslant \varphi \leqslant -0.6500$. For simplicity, we use Period (uppercase P) for the period (number of maxima per cycle) of the full MMOs and period (lowercase p) for the period (number of distinct small amplitude maxima per cycle) of the small amplitude excursions. In Figs. 2(c) and 2(d) the period doubles through the sequence 1, 2, 4, 8, 16, ..., finally leading to chaos as φ increases, while the corresponding Periods are 6, 12, 24, 48, 96, ... and chaos for the MMOs. We explore this behavior further by looking at the time series and phase portraits during the period-doubling sequence.

In most MMOs studied to date, SAOs are more frequent than LAOs, and parameter variation typically leads to a sequence of n-period-adding bifurcations such as 1^1, 1^2, 1^3, ... Here, as we vary φ from -0.6688 to -0.6500, we find an M-period-adding sequence from 5^1 to 9^1. On looking more closely at the 5^1 oscillations, we observe PD in the amplitude of the SAOs as φ increases, while the 5^1 structure and the amplitude of the LAOs are maintained.

Figures 3(a)–3(f) show time series and phase portraits obtained for increasing φ. At $\varphi = -0.66830$ [Figs. 3(a), 3(d) and 3(g)], oscillator 2 displays 5^1 MMOs with five successive LAOs followed by one small excursion, and this sequence repeats periodically, resulting in Period-6/period-1 oscillations. Oscillators 1 and 3 display nearly period-1 relaxation oscillations, though careful observation reveals that the phase difference between them shifts over the course of an MMO, i.e., the interspike interval is not constant. At slightly larger φ, the orbit diagram in Fig. 2(c) shows a period-2 oscillation for the SAOs. Figures 3(b) and 3(e) show the time series and phase portraits at $\varphi = -0.66820$. The time series show period-2 SAOs and the corresponding Period-12 MMOs. Although the number of LAOs remains unchanged, the MMO Period doubles because of the alternation in the amplitude of the SAOs. Figures 3(c) and 3(f) show period-4 (Period-24) behavior at $\varphi = -0.66812$. Figures 3(g) and 3(h) show 3D plots of the Period-6 and Period-12 MMOs (see videos 1 and 2 in the Supplemental Material [37]). On increasing φ further, we observe additional period doublings, up to period-32, followed by a region of chaos, which we investigate in more detail below.

Beyond the 5^1 chaotic MMOs, at a slightly higher φ [see Fig. 2(b)], the number of LAOs per cycle increases. We observe 6^1, 7^1, 8^1, and 9^1 MMOs, as shown in Figs. 4(a), 4(c), 4(d), and 4(e), respectively.

Above about $\varphi = -0.648264$, oscillator 2 returns to LAOs in-phase with oscillators 1 and 3 [Fig. 4(f)], and this state

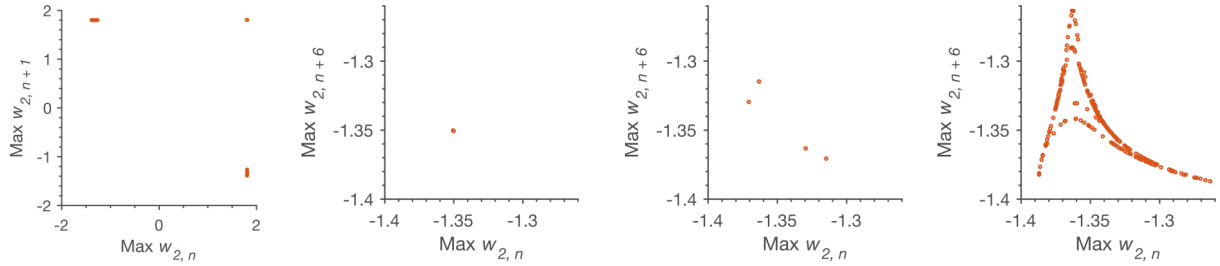

FIG. 5. Next-amplitude maps for oscillator 2. Parameters and initial conditions: same as Fig. 2. (a) Chaos, w_{n+1} *vs.* w_n with $\varphi = -0.668059$. (b) w_{n+6} *vs.* w_n showing period-1 (Period-6) with $\varphi = -0.66830$. (c) w_{n+6} *vs.* w_n showing period-4 (Period-24) at $\varphi = -0.66812$. (d) w_{n+6} *vs.* w_n displaying chaos $\varphi = -0.668059$.

persists as φ is increased for the range of φ studied in this work.

To characterize the chaotic nature of the SAOs, we calculate next-amplitude (1D) maps and Lyapunov characteristic exponents for the chaotic attractor. We use the parameters and initial conditions in Fig. 2. The next-amplitude maps plot the $n+1$st maximum of w_2 against the nth maximum. Figure 5(a) shows a next-amplitude map corresponding to a chaotic time series with $\varphi = -0.668059$. The single point at the top right-hand corner corresponds to the five instances in each cycle when an LAO is followed by another LAO. The line of points at the upper left is generated by SAOs followed by an LAO, and that at the lower right by LAOs that are followed by an SAO. For periodic MMOs of period-n (Period-6n), each of the two lines would be replaced by n points. It is somewhat more instructive to focus on the SAOs alone, since this is where the PD and chaos are clearly seen. The remaining plots in Fig. 5 show maximum $w_{2,\,n+6}$ *vs.* maximum $w_{2,\,n}$, where n is chosen so that the nth peak is an SAO. With this view, the period-1 (Period-6) simple MMO seen in Figs. 3(a) and 3(d), appears as a single point in Fig. 5(b). Similarly, the period-4 (Period-24) MMO gives four points [Fig. 5(c)] in the next-amplitude map. At $\varphi = -0.668059$, where the amplitude of the SAOs is chaotic, the next-amplitude map in Fig. 5(d) gives well-defined curves with four peaks that occur around the same value of Max w_2, n. Most chaotic oscillators display quadratic maps with only a single maximum. We do not have a full understanding of the multipeak structure seen in Fig. 5(d), but note that (i) the qualitative appearance of the next-amplitude maps of the chaotic MMOs repeatedly shifts between segmented single-peak maps and multipeak maps like that in Fig. 5(d) over narrow ranges of φ; (ii) the multipeak structure may be a shadow of the banded chaos seen for some values of φ; and (iii) these maps show the behavior of a single variable in a six-dimensional space and thus constitute a projection of a more complex object.

TABLE I. Feigenbaum constants for Case 1 (Table III).

Period, n	φ	F_N
1	−0.668264000	
2	−0.668132000	
4	−0.668104900	4.870848708
8	−0.668099400	4.927272727
16	−0.668098220	4.661016949

The spectrum of Lyapunov characteristic exponents measures the degree of convergence or divergence of nearby trajectories. For a chaotic attractor, we expect one zero (or near-zero) exponent, corresponding to motion along the attractor, and one (or more) positive exponent(s) corresponding to the divergence of neighboring trajectories characteristic of chaotic behavior. We calculated the spectrum of Lyapunov exponents, λ_i, for the six-dimensional phase space of Eq. (1) using parameters from Fig. 5(d) with the method of Ref. [38] and obtained, $\lambda_1 = 8.120 \times 10^{-4}$, $\lambda_2 = -2.400 \times 10^{-5} (\approx 0)$, $\lambda_3 = -4.106 \times 10^{-3}$, $\lambda_4 = -1.972$, $\lambda_5 = -4.233$, and $\lambda_6 = -6.147$. The spectrum of Lyapunov exponents with $\varphi = -0.69$ [Region III of Fig. 2(a)] is $\lambda_1 = -5.000 \times 10^{-6} (\approx 0)$, $\lambda_2 = -1.722 \times 10^{-3}$, $\lambda_3 = -5.058 \times 10^{-3}$, $\lambda_4 = -4.241$, $\lambda_5 = -4.246$ and $\lambda_6 = -4.249$. The lack of a positive Lyapunov exponent and the presence of a Lyapunov exponent that is close to zero suggests that the system evolves periodically in this regime.

A characteristic feature of chaotic systems is the presence of periodic windows separating chaotic bands in the orbit diagram. For a class of maps including the logistic map, these periodic windows occur in a universal sequence (the U sequence) in the order 6, 5, 3, 2×3, 5, 6 [39]. The periodic windows 6, 5, 3 correspond to large windows after the initial chaotic oscillations, with the 2×3 window representing the first PD in the period-3 window [40]. The orbit diagrams shown in Figs. 2(c)–2(d), are similar but more complex. Figures 2(e)–2(f) illustrate the fractal-like structure that appears as the branches split further and then recombine at large φ, interrupted by regions of simple periodic LAOs.

Another feature common to systems with a PD route to chaos is a universal constant known as the Feigenbaum constant (F_N). For a class of systems that display PD, the ratio of distances between successive bifurcation points converges to the transcendental number 4.669 . . . [41]. We calculated the Feigenbaum constant for the 5^1 PD-MMOs using Eq. (2) and obtained the results shown in Table I. We limit the results to period-16 because the exact location of the bifurcation becomes difficult to determine for higher values of n.

$$F_N = \lim_{n\to\infty} \frac{\varphi_{n+1} - \varphi_n}{\varphi_{n+2} - \varphi_{n+1}}. \tag{2}$$

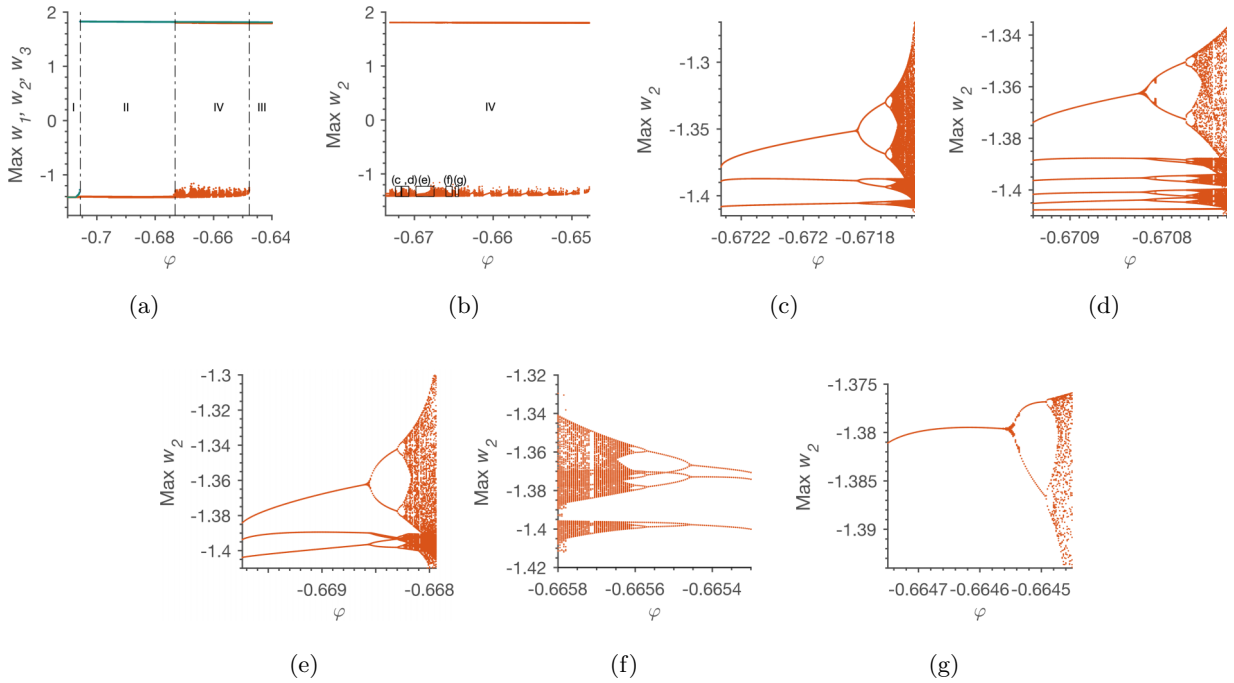

FIG. 6. Orbit diagrams showing maximum amplitude of oscillations with varying φ. Parameters and initial conditions as with Fig. 2. (a) All three oscillators. (b) Oscillator 2. (c) 7^3 MMOs with increasing φ. (d) $7^3 8^3$ MMOs with increasing φ. (e) 8^3 MMOs with increasing φ. (f) 8^3 MMOs with decreasing φ. (g) 15^1 MMOs with increasing φ. Figures 6(c)–6(g) show only the small amplitude oscillations. Blue: oscillator 1, red: oscillator 2, green: oscillator 3. Where the blue, red and green trajectories overlap, only green is seen. Similarly, only green is seen where blue and green trajectories intersect.

We also examined the effect of varying ε, keeping all other parameters and initial conditions in Fig. 2 constant with $\varphi = -0.668059$. We found that by increasing ε in the range $0.10645 \leqslant \varepsilon \leqslant 0.2169$, we generated the same sequence of period doubling leading to chaos in the 5^1–9^1 MMOs that we found by varying φ at fixed ε (Fig. 14). We also obtained 10^1 MMOs by varying ε, a pattern that we did not observe when varying φ at fixed ε.

TABLE II. Notable observations for MS system.

Case	Range of φ	MMOs in Region IV	PD
1	-0.67226 to -0.67160	7^3	Increasing
2	-0.67094 to -0.67065	7^3, 8^3	Increasing
3	-0.66976 to -0.66805	8^3	Increasing
4	-0.66580 to -0.66545	8^3	Decreasing
5	-0.66477 to -0.66440	15^1	Increasing
6	-0.66300 to -0.66240	16^1	Increasing
7	-0.66200 to -0.66180	$16^1 17^1$	Increasing
8	-0.66120 to -0.66020	17^1	Increasing
9	-0.65983 to -0.65960	$17^1 18^1$	Increasing
10	-0.65892 to -0.65800	18^1	Increasing
11	-0.65750 to -0.65720	$18^1 19^1$	Increasing
12	-0.65640 to -0.65560	19^1	Increasing
13	-0.65479 to -0.65460	$19^1 20^1$	Increasing
13	-0.65380 to -0.65280	20^1	Increasing
14	-0.65180 to -0.65160	$20^1 21^1$	Increasing
15	-0.65060 to -0.64980	21^1	Increasing
16	$-0.64930 \leqslant$	1^0	–

We studied the influence of the other parameters on the dynamics as well. As shown in Table IV (Fig. 14), all the parameters show the signature MMOs. Varying h and D_w gives PD-MMOs and period-adding bifurcations as the parameter decreases. The D_w sequence shows 10^1 and 11^1 in addition to the 5^1–9^1 MMOs.

The results described thus far were obtained with a single set of initial conditions. In an effort to assess the robustness of the observed behavior, we explored a number of other initial conditions. The results are described in detail in the Appendix. As shown in Table III and Fig. 12, the PD-MMO route to chaos occurs for a variety of initial conditions. In particular, it appears to be necessary, though not sufficient, for oscillators 1 and 3 to have a significant initial phase difference in order for this behavior to occur. If the two outer oscillators are too close to one another initially, no MMOs arise. Similarly, even for a wide separation of oscillators 1 and 3, certain initial positions of oscillator 2 lead to simple in-phase LAOs (cf. Cases 14 and 15 of Table III and Fig. 12).

B. Master-slave system

The above observations suggest that the forcing of the central oscillator by the biphasic signal of the nearly antiphase outer oscillators may play a crucial role. We therefore studied a master-slave-like forced system, in which the outer two oscillators 1 and 3 force the middle oscillator, 2 by setting $D_w = 0$ in the second and sixth equations of Eq. (1) as shown in Fig. 1(b). With this configuration, the outer oscillators are decoupled from one another. This modified system showed a richer set of MMOs with PD than those found in the fully

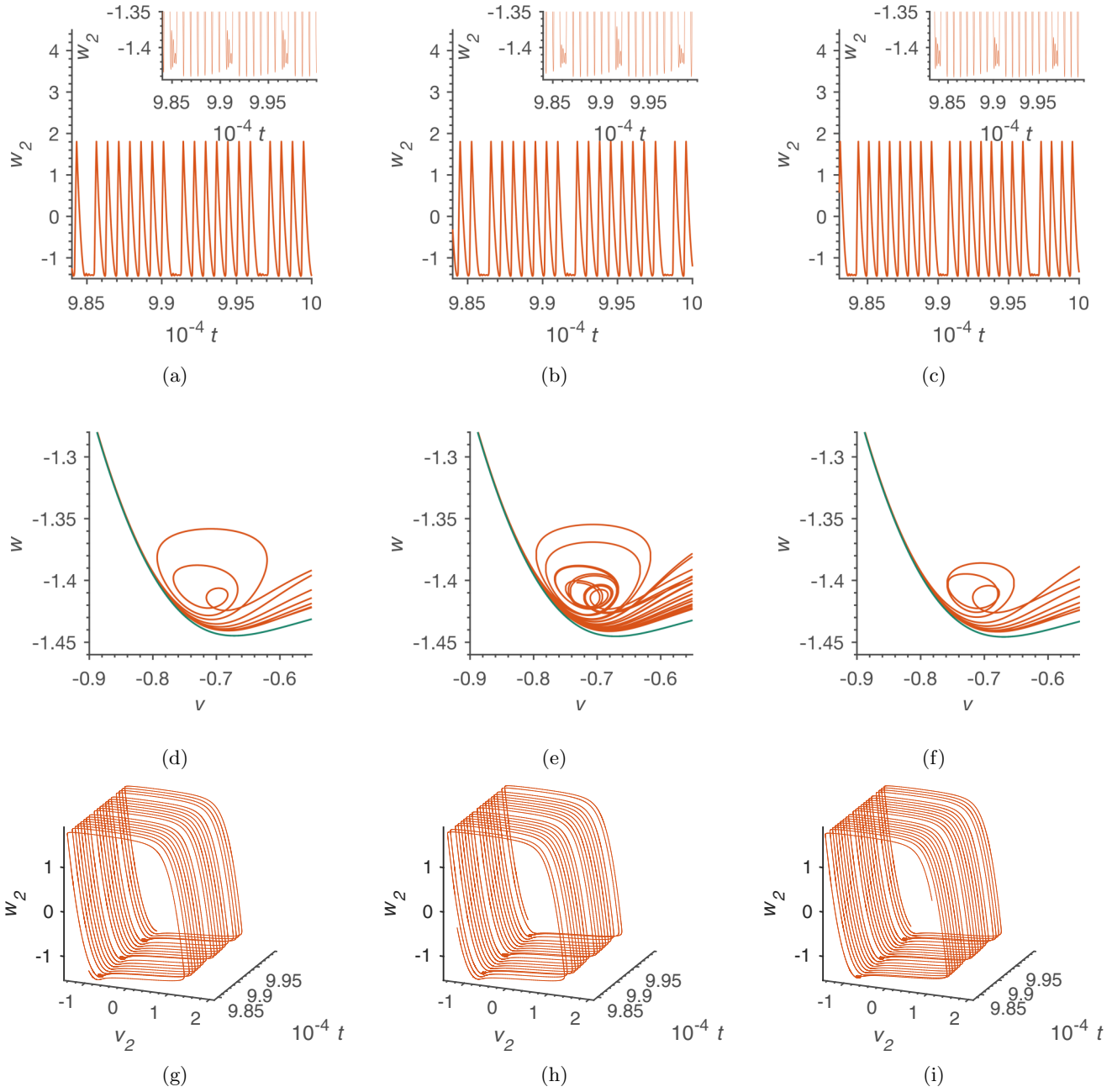

FIG. 7. Time series and phase portraits of oscillator 2 from numerical simulations of the master-slave system. Parameters and initial conditions are the same as Fig. 2. Top: time series; middle panel: phase portraits; bottom panel: 3D plot of v_2, w_2 vs. time. (a), (d), (g) 7^3 MMOs at $\varphi = -0.67226$. (b), (e), (h) $7^3 8^3$ MMOs with period-3 at $\varphi = -0.67092$. (c), (f), (i) 8^3 MMOs with period-3 at $\varphi = -0.66976$. For the phase portraits, blue: oscillator 1, red: oscillator 2, green: oscillator 3. Only green is seen where the blue, red, and green trajectories overlap. Similarly, only green is seen where blue and green trajectories intersect.

coupled system. For example, we observed 7^3, $7^3 8^3$, and 8^3 MMOs with PD sequences to chaos, as shown in Table II and Fig. 7. Thus, we observed a single period-adding bifurcation from 7^3 to 8^3 MMOs. The orbit diagrams [see Figs. 6(c)–6(f)] show these MMOs. The orbit diagram in Fig. 6(c) begins with three small and one large maximum. The latter, which corresponds to the seven large amplitude peaks, is outside the range of the figure. Each of the three small maxima undergoes a PD sequence to chaos, while the large maxima stay the same. We did not observe this behavior with the full system. We decided to explore this region further. Case 1 of Table II shows 7^3 MMOs that correspond to the orbit diagram in Fig. 6(c). The time series [Fig. 7(a)], phase portraits [Fig. 7(d)], and 3D plots [Fig. 7(g)] display three small excursions followed by seven large excursions, corresponding to period-3 SAOs. As φ increases, we observe a $7^3 8^3$ pattern, characterized by alternation of 7^3 and 8^3 MMOs, as shown in the time series in Fig. 7(b). Because each period consists of two MMOs with different amplitudes for the small maxima (and different numbers of LAOs), these MMOs contain six SAOs initially,

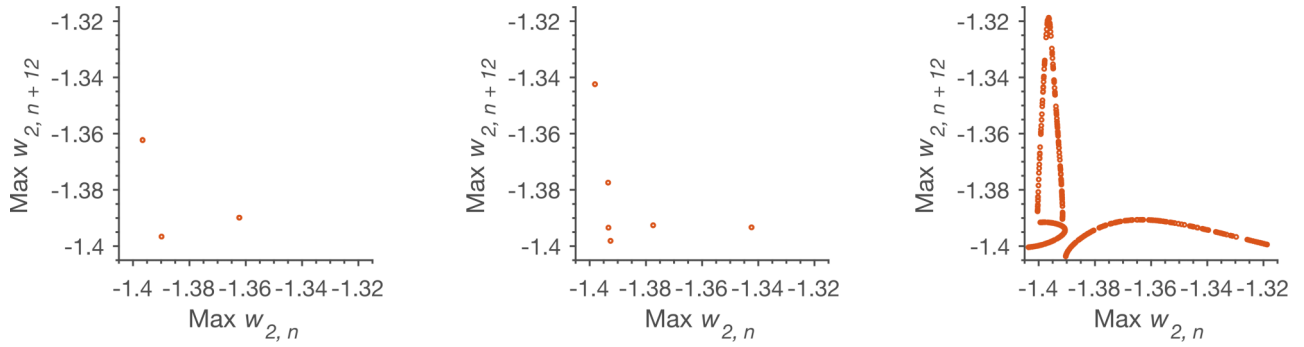

FIG. 8. Next-amplitude (1D) maps of 8^3 MMOs for oscillator 2 from numerical simulations for the master-slave system. Parameters and initial conditions are the same as Fig. 2. (a) Map with period-3 at $\varphi = -0.668589$. (b) Map with period-6 at $\varphi = -0.668305$. (c) Chaos at $\varphi = -0.66805$.

followed by 12, 24,... during the PD sequence, eventually becoming chaotic as φ increases. The orbit diagram for the SAOs in Fig. 6(d) illustrates this behavior. Figure 6(f) exhibits an 8^3 PD route to chaos with decreasing φ. Also, the number of LAOs before a single SAO increased in the master-slave scenario. Instead of the 5^1–9^1 MMOs with PD seen in the full system, the master-slave system displays 15^1–21^1 MMOs with PD (see Table II). We conclude that the forcing of the central oscillator by the outer ones plays a key role in inducing the MMO/PD behavior.

An 8^3 MMO [see Figs. 7(c), 7(f), and 7(i)] with PD as φ increases was observed after the 7^38^3 pattern as shown in Case

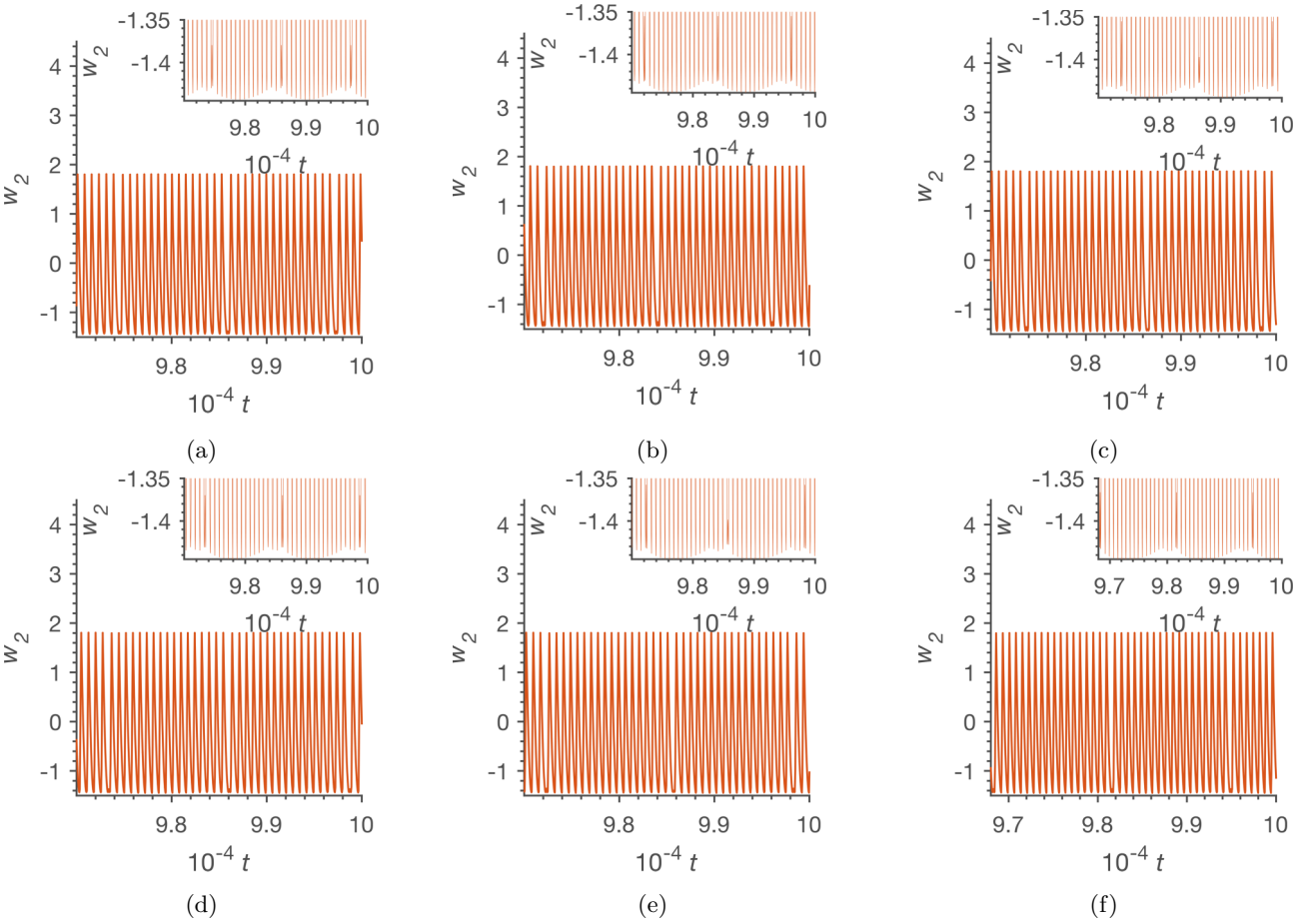

FIG. 9. Time series of oscillator 2 from numerical simulations. Parameters and initial conditions are the same as Fig. 2. (a) 15^1 MMOs at $\varphi = -0.6647$. (b) 16^1 MMOs at $\varphi = -0.6627$. (c) 16^117^1 MMOs at $\varphi = -0.6619$. (d) 17^1 MMOs at $\varphi = -0.6608$. (e) 17^118^1 MMOs at $\varphi = -0.6597$. (f) 18^1 MMOs at $\varphi = -0.6585$.

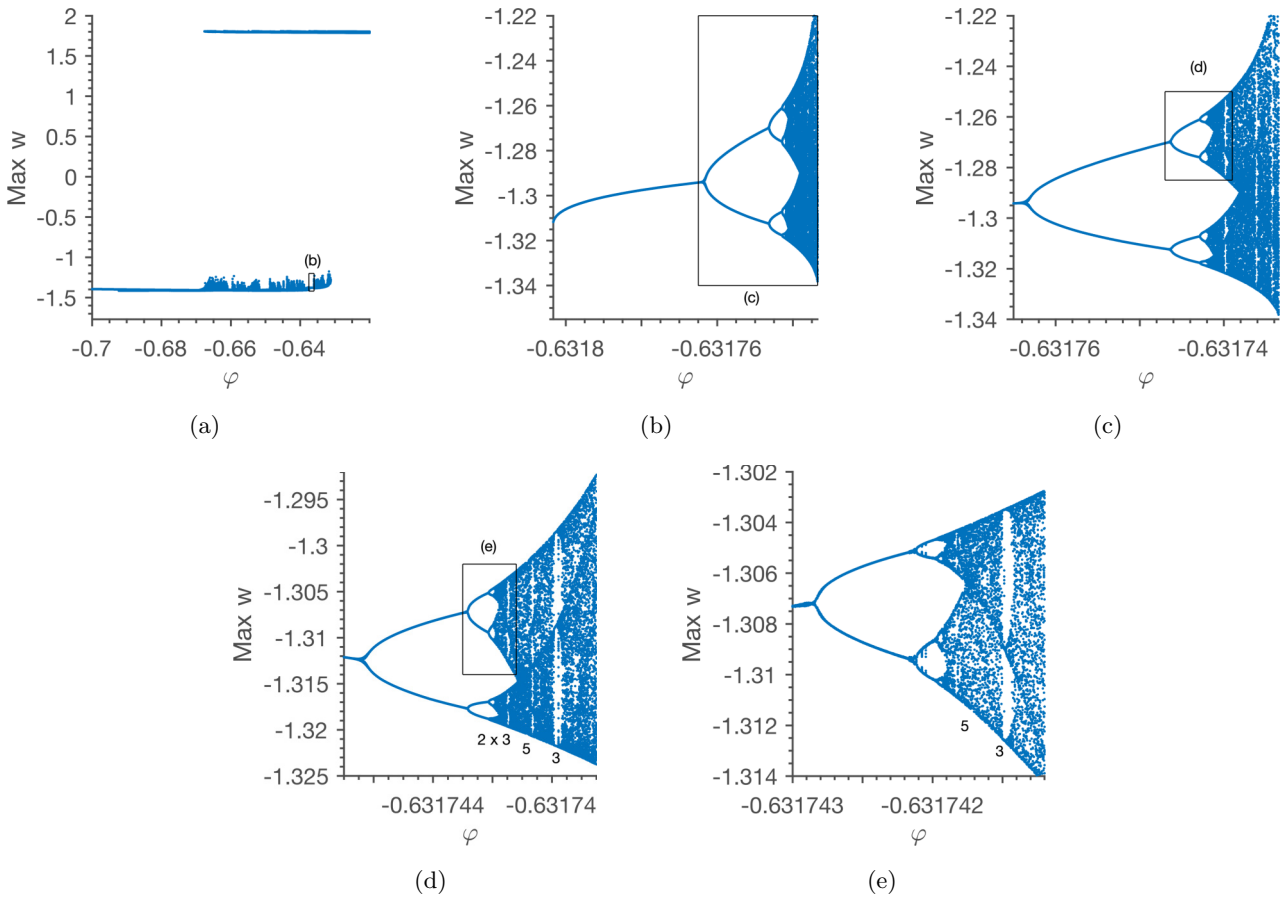

FIG. 10. Orbit diagrams showing maximum amplitude of oscillations of the uncoupled forced system with varying φ. Parameters: $A = 3.378$, $B = 0.112$, $\varepsilon = 0.1335$, $h = 2.0$, $a = 3.0$, $\omega = 2\pi/T$, $T = 378$, $D_w = 1.865 \times 10^{-3}$ with $\theta = \pi/2$ and initial conditions $(v,\ w) = (0.97553,\ 1.14483)$. (a) Full orbit diagram. (b) Blowup from Fig. 10(a) for the 5^1 MMOs. (c) Blowup from Fig. 10(b). (d) Blowup from Fig. 10(c). (e) Expanded from Fig. 10(d).

3 of Table II. The orbit diagram 6(e) for this MMO is similar to the one observed with the 7^3 MMOs. The 7^3 and 8^3 MMOs constitute another period-adding bifurcation not seen with the full reciprocally coupled system.

At higher φ, we observe a second PD sequence to chaos involving the 8^3 MMOs. This PD, however, occurs with decreasing φ, as shown in the orbit diagram in Fig. 6(f).

We also calculated the next-amplitude (1D) maps of the 7^3 and 8^3 MMOs, as well as that of 7^38^3 MMOs, where the cycle contains both MMOs. Figure 8(a) shows the map for period-3 8^3 MMOs, followed by doubling to period-6, as shown in Fig. 8(b). As the 8^3 MMOs become chaotic, we observe a 1D map consisting of three disjoint segments, shown in Fig. 8(c).

On increasing φ, we observe MMOs similar to those seen in the full system, but with a higher number of large-amplitude excursions before a single small excursion. For example, the first pattern we observe after the 8^3 MMOs consists of 15^1 MMOs [Figs. 6(g) and 9(a)]. Various MMOs (15^1–21^1 MMOs) with PD are seen, as shown in Table II. During the transition from one type of MMO to another, we observe MMOs consisting of a combination of the previous and next MMOs. For example, in Table II, we find 16^117^1 MMOs (Case 7) between 16^1 MMOs (Case 6) and 17^1 MMOs (Case 8). The same pattern is seen with all the transitions. Figures 9(a)–9(f) show some of the time series for the 15^1–18^1 MMOs.

C. Uncoupled forced system

To gain further insight into the occurrence of MMOs and its relation to the initial phase separation between the outer oscillators, we simplified the master-slave system further, to a single van der Pol oscillator forced by two sine functions with a phase difference θ, as shown in the scheme in Fig. 1(c) and Eq. (3)

$$\begin{aligned}\frac{dv}{dt} &= -hv^3 + av - w,\\ \frac{dw}{dt} &= \varepsilon(v-\varphi) + D_w\left(-2w + \frac{A}{2}[\sin(z) + \sin(z+\theta)] + B\right),\\ \frac{dz}{dt} &= \omega.\end{aligned} \tag{3}$$

where A is the amplitude of the forcing, θ is the phase difference, $\omega = 2\pi/T$ is the forcing frequency with period T, and B is an offset. A, B, θ and ω are chosen to make the perturbation resemble the effect of the outer oscillators in the coupled system.

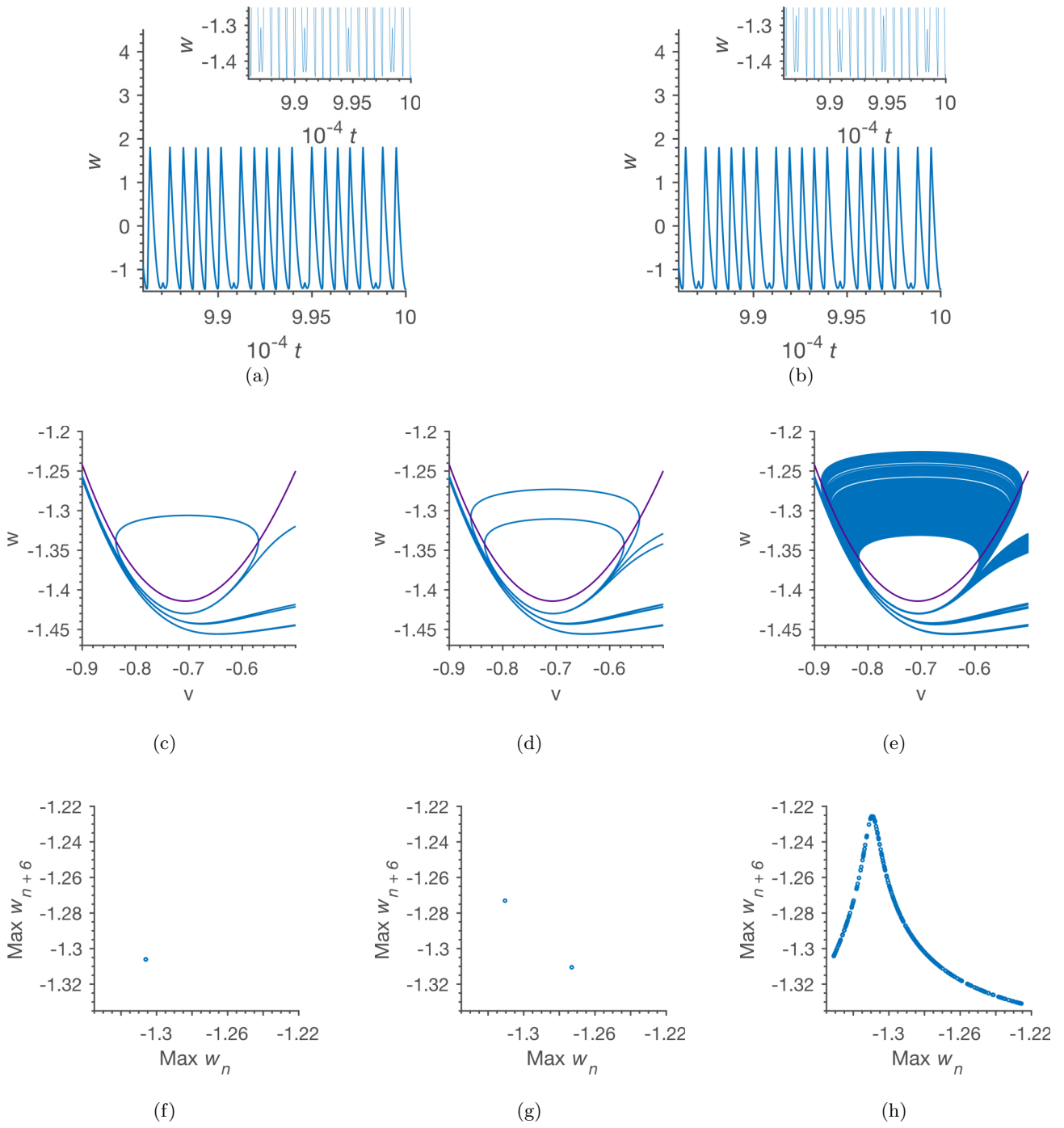

FIG. 11. Numerical simulations of 5^1 MMOs in the uncoupled forced system. Parameters and initial conditions same as in Fig. 10. Top: time series, middle: phase portraits, bottom: next-amplitude (1D) maps. (a), (c), (f) Period-6 MMOs at $\varphi = -0.631800$. (b), (d), (g) Period-12 at $\varphi = -0.631750$. (e), (h) Chaos at $\varphi = -0.631735$. Purple: v nullcline.

We numerically integrated Eq. (3), keeping h, a, ε and D_w at the same values used for both the fully coupled and the master-slave systems, and with $A = 3.378$ and $B = 0.112$. We first studied the behavior of the system with $\theta = \pi/2$.

We observe several scenarios similar to those seen in the master-slave system. The orbit diagram in Fig. 10 contains three different regions as φ increases. In Region I, we obtain SAOs, followed by Region IV, where we observe several MMOs as φ increases. At high values of φ, the system displays only LAOs. We focus on the MMOs.

As φ increases, before the system transitions to simple LAOs, the oscillator goes through 5^1 MMOs that exhibit PD to chaos, as shown in the orbit diagrams in Figs. 10(b)–10(c). We explore the time series, phase portraits and next-amplitude (1D) maps of the forced system and compare them to the fully coupled system and the master-slave system.

For $\theta < \pi$, as φ increases, various MMOs appear, some with simple periodicity in the SAOs similar to those observed in the fully coupled system (e.g., 5^1 MMOs, as

TABLE III. Observations made with different initial conditions.

Case	Initial conditions	MMOs in Region IV	Oscillator 2	Comments
1	$(v_1, w_1) = (-0.624209340312539\ -1.31378200470845)$ $(v_2, w_2) = (0.1563555683989080\ 1.791056306867020)$ $(v_3, w_3) = (0.9755267396515510\ 1.144833731651560)$	5^1, 6^1, 7^1, 8^1, 9^1	Right branch	Osc. 1 close to minimum and Osc. 3 on rightmost branch
2	$(v_1, w_1) = (0.1563555683989080\ 1.791056306867020)$ $(v_2, w_2) = (-0.624209340312539\ -1.31378200470845)$ $(v_3, w_3) = (0.9755267396515510\ 1.144833731651560)$	8^1, 9^1	Close to the minimum of cubic nullcline	1 and 3 on Oscs[a]. the rightmost branch of cubic nullcline
3	$(v_1, w_1) = (-0.624209340312539\ -1.31378200470845)$ $(v_2, w_2) = (0.9755267396515510\ 1.144833731651560)$ $(v_3, w_3) = (0.1563555683989080\ 1.791056306867020)$	5^1, 6^1, 7^1, 8^1, 9^1	Right branch	Osc. 1 close to minimum and Osc. 3 on rightmost branch
4	$(v_1, w_1) = (-1.26150618922426\ 0.227037058153444)$ $(v_2, w_2) = (-0.712563911545149\ -1.41430735700971)$ $(v_3, w_3) = (-0.00948127333826656\ -1.39291991672867)$	5^1, 6^1, 7^1, 8^1, 9^1	Close to the minimum of cubic nullcline	Osc. 1 on leftmost branch and Osc. 3 jumping to the rightmost branch
5	$(v_1, w_1) = (-0.735283410089882\ -1.29726550687495)$ $(v_2, w_2) = (0.949247645832642\ 1.14855231424957)$ $(v_3, w_3) = (0.188699586139167\ 1.78261121012471)$	5^1, 6^1, 7^1, 8^1, 9^1	Right branch	Oscs. 1 and 3 at opposites ends of the cubic nullcline
6	$(v_1, w_1) = (-0.735283410089882\ -1.29726550687495)$ $(v_2, w_2) = (0.949247645832642\ 1.14855231424957)$ $(v_3, w_3) = (-0.735283410089882\ -\ 1.29726550687495)$	1^0	Right branch	Oscs. 1 and 3 together and at or close to the minimum of cubic nullcline
7	$(v_1, w_1) = (0.188699586139167\ 1.78261121012471)$ $(v_2, w_2) = (0.949247645832642\ 1.14855231424957)$ $(v_3, w_3) = (0.188699586139167\ 1.78261121012471)$	1^0	Right branch	Oscs. 1 and 3 together and close to the maximum of cubic nullcline
8	$(v_1, w_1) = (-0.735283410089882\ -1.29726550687495)$ $(v_2, w_2) = (-0.735283410089882\ -1.29726550687495)$ $(v_3, w_3) = (0.188699586139167\ 1.78261121012471)$	5^1, 6^1, 7^1, 8^1, 9^1	Close to the minimum of cubic nullcline	Oscs. 1 and 2 together and at or close to the minimum of cubic nullcline
9	$(v_1, w_1) = (-0.735283410089882\ -1.29726550687495)$ $(v_2, w_2) = (0.188699586139167\ 1.78261121012471)$ $(v_3, w_3) = (0.188699586139167\ 1.78261121012471)$	5^1, 6^1, 7^1, 8^1, 9^1	Right branch	Oscs. 2 and 3 together and close to the maximum of cubic nullcline
10	$(v_1, w_1) = (-1.43816005927240\ 1.62755439706495)$ $(v_2, w_2) = (0.946935061495364\ 1.17197142977014)$ $(v_3, w_3) = (-0.853464256410909\ -1.31926341380611)$	5^1, 6^1, 7^1, 8^1, 9^1	Right branch	Oscs. 1 and 3 on extremes of the leftmost branch of cubic nullcline
11	$(v_1, w_1) = (-1.438160059272400\ 1.627554397064950)$ $(v_2, w_2) = (-0.637628110091284\ -1.39329060779399)$ $(v_3, w_3) = (-0.853464256410909\ -1.31926341380611)$	5^1, 6^1, 7^1, 8^1, 9^1	Close to the minimum of cubic nullcline	Oscs. 1 and 3 on extremes of the leftmost branch of cubic nullcline
12	$(v_1, w_1) = (-1.43816005927240\ 1.62755439706495)$ $(v_2, w_2) = (0.946935061495364\ 1.17197142977014)$ $(v_3, w_3) = (-1.22523528881125\ -0.00298801650949941)$	5^1, 6^1, 7^1, 8^1, 9^1	Right branch	Osc. 1 on top of extreme and osc. 3 midway of the of the leftmost branch
13	$(v_1, w_1) = (-1.43816005927240\ 1.62755439706495)$ $(v_2, w_2) = (0.946935061495364\ 1.17197142977014)$ $(v_3, w_3) = (-1.39018633830603\ 1.19604888440157)$	1^0	Right branch	Osc. 1 and 3 close to each other and close to top of extreme left branch
14	$(v_1, w_1) = (0.839121121928404\ 1.45232550993826)$ $(v_2, w_2) = (-1.39018633830603\ 1.19604888440157)$ $(v_3, w_3) = (1.38707481920313\ -1.16194692466634)$	5^1, 6^1, 7^1, 8^1, 9^1	Left branch	Osc. 1 and 3 on extreme ends of rightmost branch of cubic nullcline
15	$(v_1, w_1) = (0.839121121928404\ 1.45232550993826)$ $(v_2, w_2) = (-0.637628110091284\ -1.39329060779399)$ $(v_3, w_3) = (1.38707481920313\ -1.16194692466634)$	6^1, 7^1, 8^1, 9^1	Close to the minimum of cubic nullcline	Oscs. 1 and 3 on extreme ends of rightmost branch of cubic nullcline
16	$(v_1, w_1) = (1.38707481920313\ -1.16194692466634)$ $(v_2, w_2) = (-0.637628110091284\ -1.39329060779399)$ $(v_3, w_3) = (-1.43816005927240\ 1.62755439706495)$	5^1, 6^1, 7^1, 8^1, 9^1	Close to the minimum of cubic nullcline	Oscs. 1 and 3 on opposite ends of the of cubic nullcline

[a]Oscillators.

shown in Fig. 11), as well as others with complex periodicity in the SAOs as shown in the time series, phase portrait and next-amplitude (1D) map in Fig. 16. Figures 11(a)–11(b) and Figs. 11(c)–11(d) show the time series and the corresponding phase portraits with Period-6 (period-1) and Period-12 (period-2), respectively. At $\varphi = -0.631735$, the oscillator displays chaotic 5^1 MMOs [Fig. 11(e)]. The next-amplitude (1D) maps show the period-doubling from one to two and finally chaos, as shown in Figs. 11(f)–11(h). The Lyapunov characteristic exponents with parameters and initial conditions from Fig. 11(h) are $\lambda_1 = 1.1580 \times 10^{-3}$, $\lambda_2 = -3.9199$, $\lambda_3 = 0.0000$. The system exhibits a U sequence similar to those observed with the fully coupled and master-slave systems.

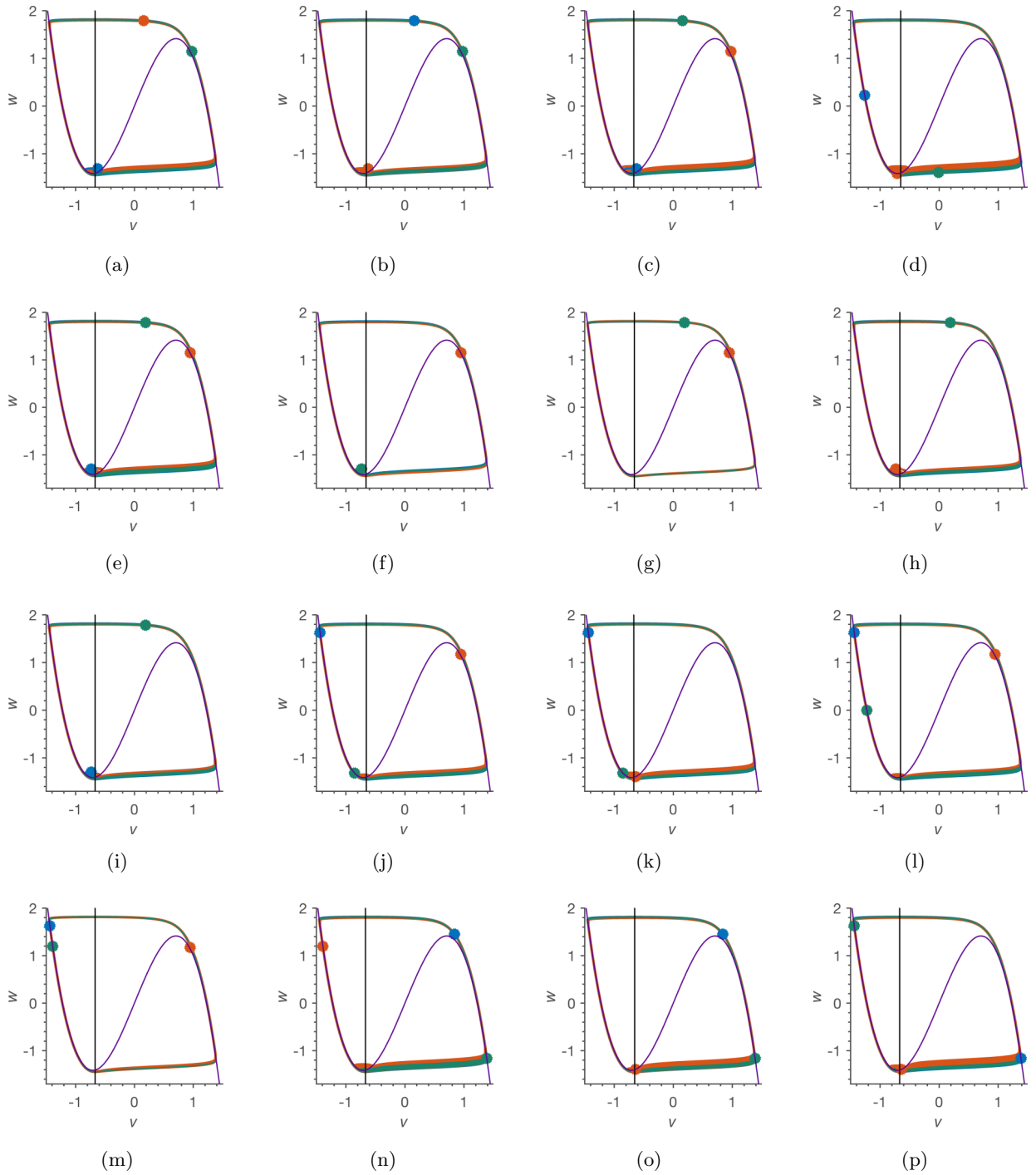

FIG. 12. Phase portraits of all three oscillators showing their initial positions (large dots). Oscillator 1, blue; oscillator 2, red; oscillator 3, green. Parameters: $a = 3.0$, $\varepsilon = 0.1335$, $h = 2.0$ and $D_w = 1.865 \times 10^{-3}$ with $\varphi = -0.6683$. (a) Case 1. (b) Case 2. (c) Case 3. (d) Case 4. (e) Case 5. (f) Case 6. (g) Case 7. (h) Case 8. (i) Case 9. (j) Case 10. (k) Case 11. (l) Case 12. (m) Case 13. (n) Case 14. (o) Case 15. (p) Case 16. Purple: v nullcline and black: w nullcline. Where blue and green trajectories intersect, only green is seen. Only red is visible when red and blue trajectories overlap. Where red and green intersect, only green is seen.

Unlike the other systems we studied, where we found multiple M^1 MMOs with PD as well as period-adding bifurcations, here only the 5^1 MMOs show PD. Instead, we found other MMOs with period-adding bifurcations with SAOs exhibiting multiperiodic or complex oscillations.

A surprising result, which differs from the behavior of the autonomous coupled system, is that at $\theta = 0$, i.e., with forcing by a single sine wave, the system exhibits $5^1(5^2)^2$ PD-MMOs (see Table VII in Appendix C).

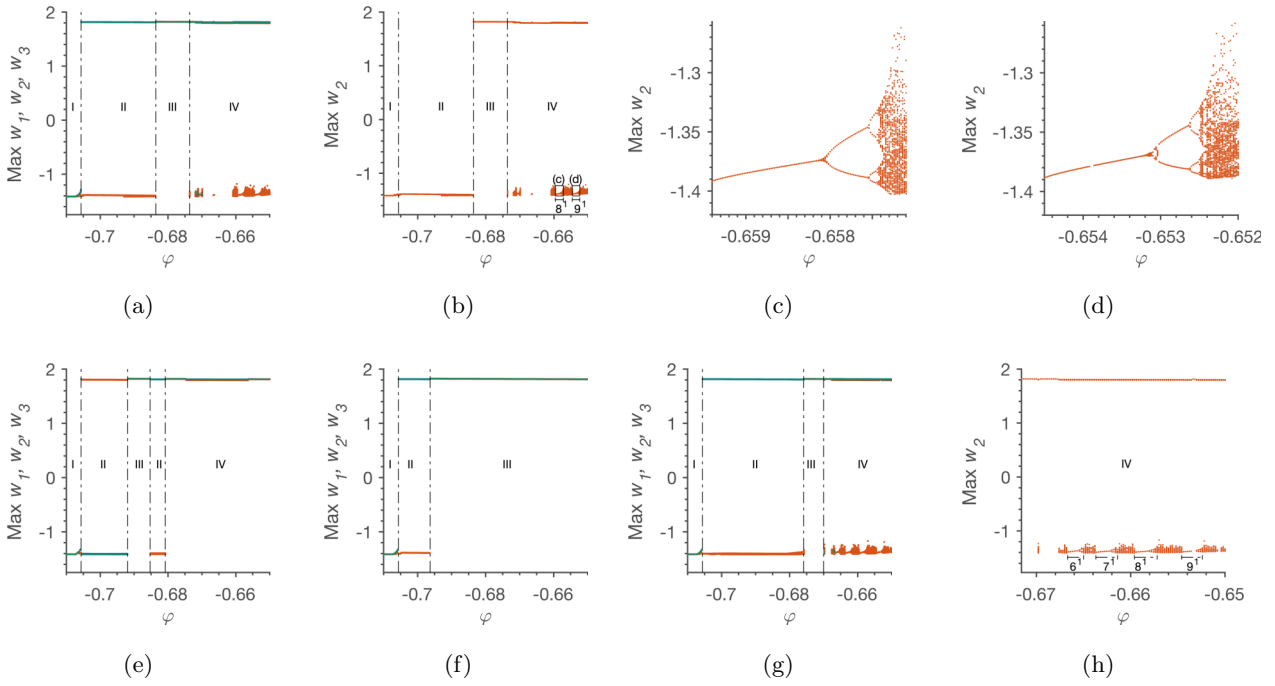

FIG. 13. Orbit diagrams showing maximum amplitude of oscillations with varying φ. (a) Case 2. (b) Case 2, Oscillator 2 only. (c) Expanded from Fig. 13(b). (d) Expanded from Fig. 13(b). (e) Case 6. (f) Case 13. (g) Case 15. (h) Oscillator 2 from Fig. 13(g).

III. CONCLUSIONS

We have observed and characterized a PD route to chaos, in which an MMO structure is preserved while period doubling leading to chaotic behavior occurs in the SAOs. Features such as the 1D map and the sequence of periodic windows in the orbit diagram of the SAOs resemble those found in previously studied chaotic systems. We attribute this phenomenon to the forcing of the central oscillator by the two outer oscillators with a sufficient phase difference between them, modulated by the indirect linkage of the outer oscillators via their coupling to the central one. In Appendix D, we examine the effect of the initial phase difference in more detail. We find that if the initial phase difference between the central oscillator and either of the outer oscillators is close to zero, PD-MMOs occur only if the initial phase difference between the outer oscillators is large (between about 0.2 and 0.8). On the other hand, if the initial phase difference between the central oscillator and one of the outer oscillators is large, PD-MMOs arise even for tiny initial phase differences between the outer oscillators, as small as $\approx 10^{-4}$. In the future we plan to explore the parameter space more widely in search of other M^n patterns that give rise to similar, or perhaps even more complex phenomena, as well as to search for similar behavior in other model oscillators. The existence of PD-MMO behavior in a single simply forced van der Pol oscillator suggests that the phenomenon is likely to be quite general. Studies of nonautonomous Bonhoeffer-van der Pol systems show that a forced system can produce period-adding bifurcations with complex nested mixed mode oscillations, including chaotic ones [42] as well as other MMOs [43]. In those investigations, which employed significantly lower amplitudes and longer frequencies of forcing relative to the autonomous LAOs than in our work, no period doubling was reported.

TABLE IV. Results for parameter variation with initial conditions from Case 1, Table III.

Parameter	Range	MMOs in Region IV	Constant parameters	Period-adding bifurcations
ε	$0.10645 \leqslant \varepsilon \leqslant 0.21690$	5^1, 6^1, 7^1, 8^1, 9^1, 10^1	$h = 2.0$, $a = 3.0$, $\varphi = -0.668059$, $D_w = 1.865 \times 10^{-3}$	Increasing ε
h	$1.8840 \leqslant h \leqslant 2.019$	9^1, 8^1, 7^1, 6^1, 5^1	$a = 3.0$, $\varepsilon = 0.1335$, $\varphi = -0.668059$, $D_w = 1.865 \times 10^{-3}$	Decreasing h
a	$2.9697 \leqslant a \leqslant 3.2031$	5^1, 6^1, 7^1, 8^1, 9^1	$h = 2.0$, $\varepsilon = 0.1335$, $\varphi = -0.668059$, $D_w = 1.865 \times 10^{-3}$	Increasing a
D_w	$(1.232 \leqslant D_w \leqslant 2.300) \times 10^{-3}$	11^1, 10^1, 9^1, 8^1, 7^1, 6^1, 5^1	$h = 2.0$, $a = 3.0$, $\varepsilon = 0.1335$, $\varphi = -0.668059$	Decreasing D_w

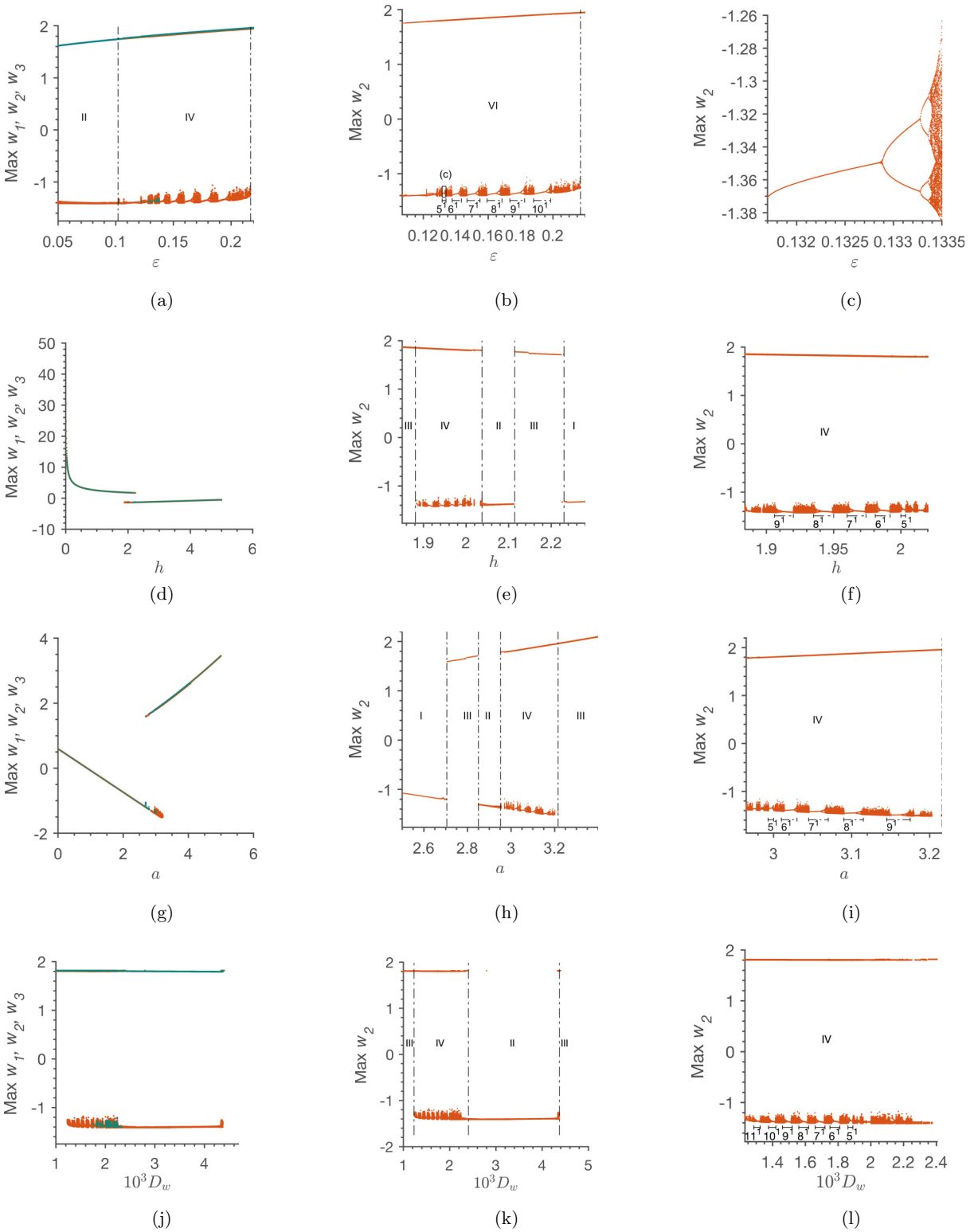

FIG. 14. Orbit diagrams showing maximum amplitude of oscillations with varying ε, h, a, and D_w with initial conditions of Case 1. Top panel: ε; middle top panel: h; middle bottom panel: a; bottom panel: D_w. (a) All three oscillators varying ε. (b) Oscillator 2. (c) Blowup from Fig. 14(b) for 5^1 MMOs. (d) All three oscillators varying h. (e) Oscillator 2 from Fig. 14(d). (f) MMOs from Fig. 14(e). (g) All three oscillators varying a. (h) Oscillator 2 from Fig. 14(g). (i) MMOs from Fig. 14(h). (j) All three oscillators varying D_w. (k) Oscillator 2 from Fig. 14(j). (l) MMOs from Fig. 14(k).

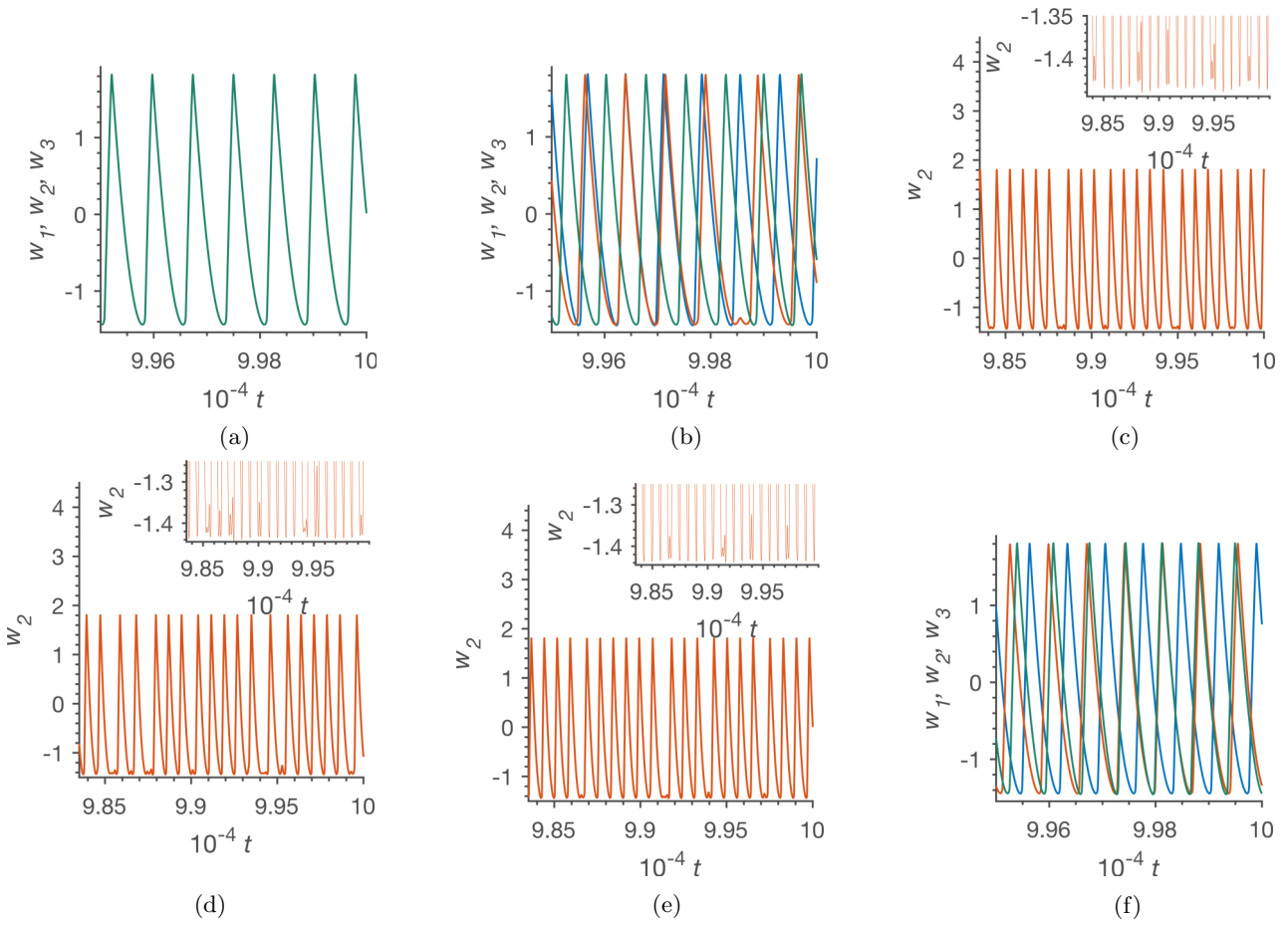

FIG. 15. Time series showing other observations made with Case 1, Table III. Parameters: $a = 3.0$, $\varepsilon = 0.1335$, $h = 2.0$, and $D_w = 1.865 \times 10^{-3}$. Initial conditions: $(v_1,\ w_1) = (-0.6242,\ -1.31378)$, $(v_2,\ w_2) = (0.15636,\ 1.79106)$, and $(v_3,\ w_3) = (0.97553,\ 1.14483)$. (a) In-phase LAOs at $\varphi = -0.6900$. (b) Out-of-phase singly periodic oscillations for oscillators 1 and 3 at $\varphi = -0.66830$. (c) Intermittent spiking observed at $\varphi = -0.668050$. (d) Intermittent spiking observed at $\varphi = -0.66770$. (e) Intermittent spiking at $\varphi = -0.66750$. (f) Out-of-phase oscillations for all three oscillators at $\varphi = -0.648264$. Blue: oscillator 1, red: oscillator 2, green: oscillator 3. Where the blue, red, and green trajectories overlap, only green is seen. Similarly, only green is seen where blue and green trajectories intersect.

IV. NUMERICAL METHODS

Numerical simulations were carried out using MATLAB ODE solver 113 for ODEs with absolute and relative tolerances of 1×10^{-9} and 1×10^{-12}, respectively. Simulations were performed with a time span of 1×10^5. All analyses of results were done after eliminating initial transients.

ACKNOWLEDGMENTS

This work was supported by the National Science Foundation under Grants No. CHE-1856484, No. DGE-1068620, and No. DMR-1420382. We thank Milos Dolnik and Jonathan Touboul for comments and suggestions.

APPENDIX A: FULLY COUPLED SYSTEM

We varied the initial conditions of the oscillators to investigate their effect on the MMOs observed. Case 1 shown in Fig. 12(a) is the focus of this paper and has been described in detail in the main text.

In Case 2 of Table III and as shown in the phase portrait in Fig. 12(a), oscillator 2 begins close to the minimum with oscillators 1 and 3 on or close to the maximum of the cubic v nullcline. We note that the only difference between Cases 1 and 2 is that the initial positions of oscillators 1 and 2 are switched. This switch between the oscillators results in the elimination of three of the MMOs with PD route to chaos found in Case 1 (5^1–7^1), as shown in Figs. 13(a) and 13(b). The 8^1–9^1 MMOs with PD route to chaos are the only ones left, as shown in Figs. 13(c) and 13(d), respectively. Thus,

TABLE V. Feigenbaum constants for MS Case 3 (Table II).

Period, n	φ	F_N
3	−0.6685896865	
6	−0.6683050794	
12	−0.6682499967	5.166905399
24	−0.6682387189	4.884170672
48	−0.6682364855	5.049610460
96	−0.6682360284	4.886020564

TABLE VI. Feigenbaum constants for MS Case 5 (Table II main text).

Period, n	φ	F_N
1	−0.6645505120	
2	−0.6644937240	
4	−0.6644845470	6.188078893
8	−0.6644825570	4.611557789
16	−0.6644821380	4.749403341
32	−0.6644820470	4.604395606

only two period-adding bifurcations remain with the switch in the initial conditions.

For Case 3, we keep oscillator 1 near the minimum (same location as Case 1) and switch the initial locations of oscillators 2 and 3. We obtain the same MMOs seen with Case 1.

Cases 1–3 involve permuting the oscillators' initial conditions. In Case 4, Fig. 12(d), we examine a new set of initial conditions. We place oscillators 2 and 3 close to the minimum and oscillator 1 midway on the leftmost branch. This arrangement results in all the MMOs seen with Case 1. For Case 5 [Fig. 12(e)], oscillator 1 is close to the minimum while oscillators 2 and 3 are placed on/or close to the maximum of the cubic nullcline. Again, we observe all MMOs with PD.

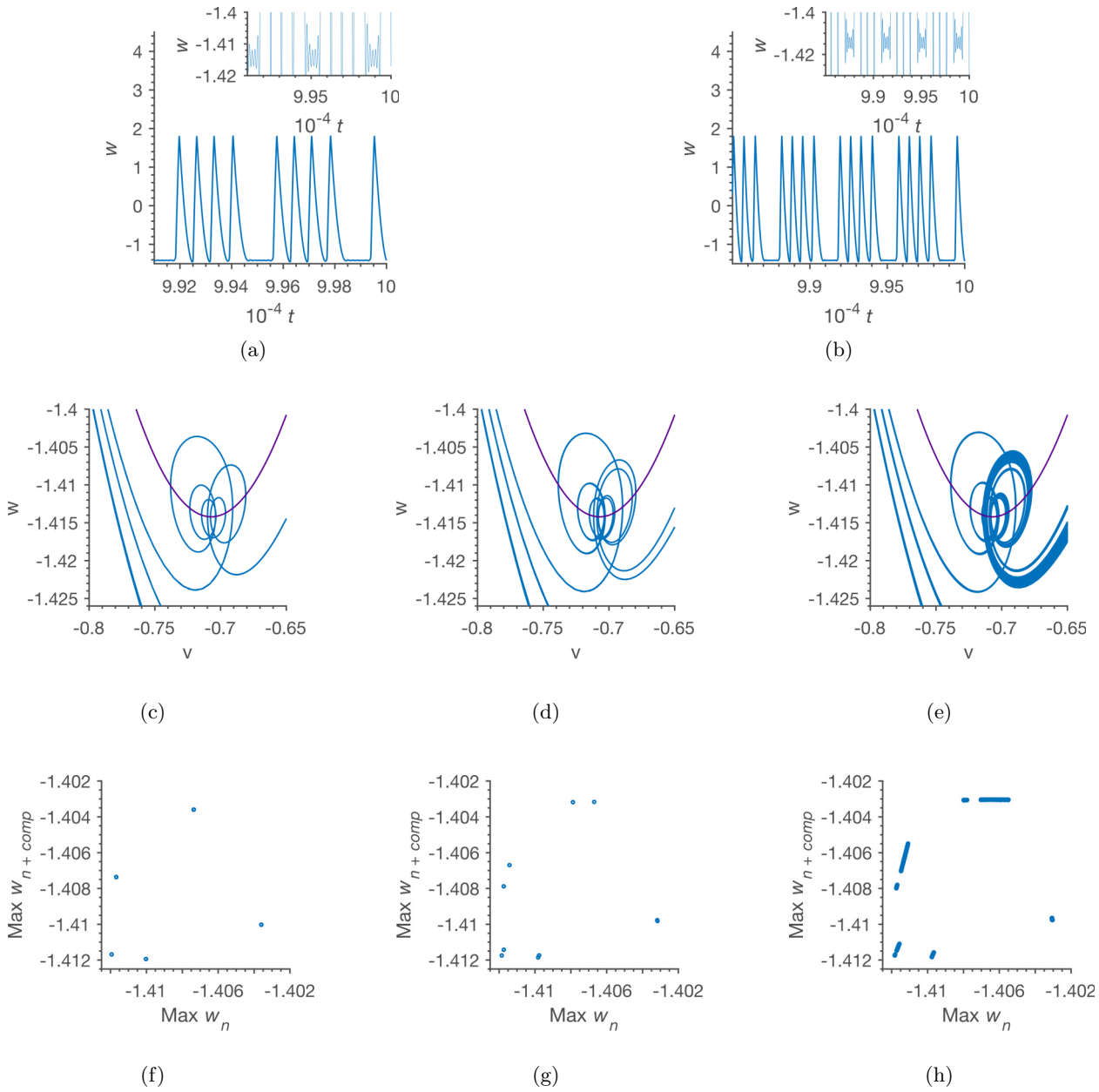

FIG. 16. Numerical simulations of the uncoupled forced system. Parameters and initial conditions as in Fig. 10. Top: time series; middle: phase portraits; bottom: next-amplitude (1D) maps. (a), (c), (f) period-1 of 4^5 MMOs at $\varphi = -0.64440$. (b), (d), (g) period-2 of 4^5 MMOs at $\varphi = -0.64397$. (e), (h) Chaos at $\varphi = -0.64385$. Purple: v nullcline.

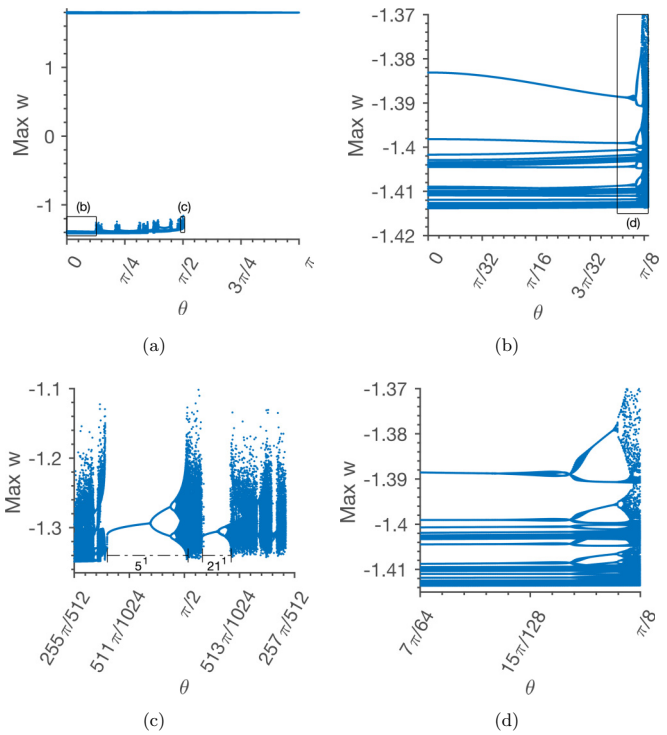

FIG. 17. Orbit diagrams showing maximum of w for the parameter θ in the uncoupled forced system. Parameters and initial conditions as in Fig. 10 (main text) with $\varphi = -0.631735$. (a) LAOs and MMOs as θ is varied. (b) Blowup from Fig. 17(a). (c) 5^1 MMOs with increasing PD expanded from Fig. 17(a). (d) Magnified view of Fig. 17(b).

For Cases 6 and 7 [Figs. 12(f) and 12(g)], we place oscillators 1 and 3 together at the same initial location at or near an extremum of the cubic nullcline. In both instances, the MMOs vanish, which suggests that sufficient separation between the outer oscillators is required to generate MMOs. The orbit diagram in Fig. 13(e) shows that, as φ is increased, oscillator 3 undergoes a symmetry breaking and starts to oscillate with small amplitude while the other two oscillators maintain their large amplitude nearly in-phase oscillations. During this stage, oscillator 3 displays triperiodic SAOs, followed by in-phase LAOs for all three oscillators and a second symmetry breaking with oscillator 2. Depending on the initial conditions, the triperiodic oscillation is followed by multiperiodic oscillations and finally chaos, as observed in our earlier work [32,33]. As shown in Fig. 13(e), there is only a single maximum in Region IV. Thus, there are no MMOs in Cases 6 and 7. At larger φ, all three oscillators resume LAOs. In Case 8 [Fig. 12(h)], oscillators 1 and 2 start off together near the minimum of the cubic nullcline with oscillator 3 at the opposite end. In Case 9 [Fig. 12(i)], we have oscillators 2 and 3 initially together close to the nullcline maximum. In both cases, we observe MMOs. Thus, initial separation between the central and outer oscillators does not appear to be necessary for the appearance of MMOs.

In Cases 10–13 [Figs. 12(j)–12(m)], we place the two outer oscillators at various locations on the left-hand branch of the cubic nullcline. Only Case 13 [Fig. 12(m)], where the outer oscillators are the closest together initially, fails to produce MMOs [see orbit diagram in Fig. 13(f)].

TABLE VII. MMOs with PD from phase difference (θ).

Case	θ	PD MMOs
1	$\pi/2$	3^{comp}, 4^{comp}, $(5^1)^3 5^2$, 5^1, 21^1
2	0	3^{comp}, 4^{comp}, $5^1(5^2)^2$, $5^1(5^2)^3$, $5^1(5^2)^4$
3	$3\pi/4$	3^{comp}, 4^{comp}, 15^1, $10^1 15^1$
4	π	–

Next we examine Cases 14–15 with oscillators 1 and 3 well separated on the rightmost branch of the v nullcline. In Case 14 [Fig. 12(n)], oscillator 2 is placed on the right-hand branch, resulting in both PD MMOs and period-adding MMOs. Case 15 [Fig. 12(o)], with oscillator 2 at the minimum of the nullcline, shows 6^1–9^1 MMOs with PD [Figs. 13(g) and 13(h)].

Lastly, we place oscillators 1 and 3 at the upper left and lower right of the cubic nullcline, respectively, with oscillator 2 near the minimum as shown in Fig. 12(p) (Case 16). We observe all MMOs with PD sequence to chaos.

We conclude that initial separation of the outer oscillators is necessary but not sufficient to produce MMOs and PD. The appearance of these phenomena also requires an appropriate initial phase relationship between the outer oscillators and the central oscillator.

We studied the effects of varying all the parameters in Eq. (1). Table IV shows some of our observations. First, we vary ε, keeping all other parameters constant, as shown in the Table and with initial conditions of Case 1. Figures 14(a)–14(b) show LAOs for oscillators 1 and 3, with oscillator 2 displaying PD MMOs as well as period-adding bifurcations (5^1–10^1). Figure 14(c) shows the PD seen with the 5^1 MMOs. The other MMO patterns exhibit similar behavior.

Next we examined the effect of varying h between 0 and 5. We obtain MMOs with PD and period-adding bifurca-

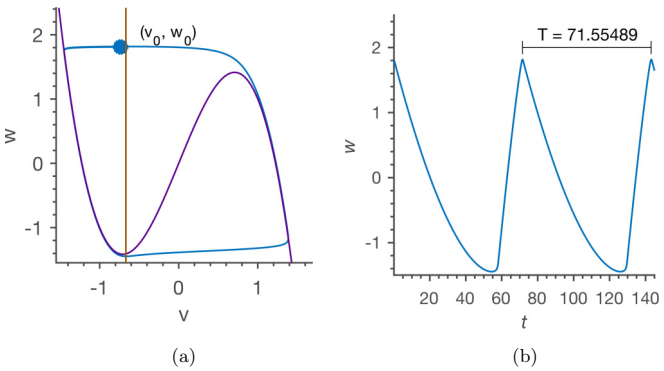

FIG. 18. Illustration of the period of uncoupled oscillator used to calculate the initial phases of the oscillators. Parameters: $a = 3.0$, $h = 2.0$, $\varepsilon = 0.1335$, and $\varphi = -0.668059$. Initial conditions: $(v,\ w) = (-0.735433,\ 1.808762)$. (a) Phase portrait. (b) Time series. Purple: v nullcline, brown: w nullcline.

TABLE VIII. Oscillators 1 and 2 kept constant, $\phi_{2,\alpha} - \phi_{1,0} = 0.76081722$, and varied oscillator 3.

Case	Initial conditions	Initial phase, $\phi_{i,\alpha} = \frac{t}{T}$	MMOs in Region IV
1	$(v_{1,0},\ w_{1,0}) = (-0.73543367,\ 1.8087622)$ $(v_{2,\alpha},\ w_{2,\alpha}) = (-0.66521082,\ -1.4463757)$ $(v_{3,\alpha},\ w_{3,\alpha}) = (-0.73543367,\ 1.8087622)$	0 0.76081722 0	1^0
2	$(v_{1,0},\ w_{1,0}) = (-0.73543367,\ 1.8087622)$ $(v_{2,\alpha},\ w_{2,\alpha}) = (-0.66521082,\ -1.4463757)$ $(v_{3,\alpha},\ w_{3,\alpha}) = (-0.73567117,\ 1.8087615)$	0 0.76081722 1.0309375×10^{-6}	1^0
3	$(v_{1,0},\ w_{1,0}) = (-0.73543367,\ 1.8087622)$ $(v_{2,\alpha},\ w_{2,\alpha}) = (-0.66521082, -1.4463757)$ $(v_{3,\alpha},\ w_{3,\alpha}) = (-0.73600866,\ 1.8087606)$	0 0.76081722 2.4959578×10^{-6}	$7^1, 8^1$ no PD to chaos
4	$(v_{1,0},\ w_{1,0}) = (-0.73543367,\ 1.8087622)$ $(v_{2,\alpha},\ w_{2,\alpha}) = (-0.66521082,\ -1.4463757)$ $(v_{3,\alpha},\ w_{3,\alpha}) = (-0.74095742,\ 1.8087461)$	0 0.76081722 2.3982862×10^{-5}	7^1 showed p-1, 8^1 showed p-1, 2.
5	$(v_{1,0},\ w_{1,0}) = (-0.73543367,\ 1.8087622)$ $(v_{2,\alpha},\ w_{2,\alpha}) = (-0.66521082,\ -1.4463757)$ $(v_{3,\alpha},\ w_{3,\alpha}) = (-0.77327807,\ 1.8086264)$	0 0.76081722 1.6462444×10^{-4}	$7^1, 8^1$ displayed p-1, 2.
6	$(v_{1,0},\ w_{1,0}) = (-0.73543367,\ 1.8087622)$ $(v_{2,\alpha},\ w_{2,\alpha}) = (-0.66521082,\ -1.4463757)$ $(v_{3,\alpha},\ w_{3,\alpha}) = (-0.83020026,\ 1.8083070)$	0 0.76081722 4.1465391×10^{-4}	7^1 showed p-1, 2, 8^1 had PD sequence to chaos.
7	$(v_{1,0},\ w_{1,0}) = (-0.73543367,\ 1.8087622)$ $(v_{2,\alpha},\ w_{2,\alpha}) = (-0.66521082,\ -1.4463757)$ $(v_{3,\alpha},\ w_{3,\alpha}) = (-1.0530435,\ 1.8054960)$	0 0.76081722 1.4772792×10^{-3}	$7^1, 8^1$ with PD sequence to chaos.
8	$(v_{1,0},\ w_{1,0}) = (-0.73543367,\ 1.8087622)$ $(v_{2,\alpha}, w_{2,\alpha}) = (-0.66521082,\ -1.4463757)$ $(v_{3,\alpha},\ w_{3,\alpha}) = (-1.2996932,\ 1.7967280)$	0 0.76081722 3.2341209×10^{-3}	$7^1, 8^1$ with PD sequence to chaos.
9	$(v_{1,0},\ w_{1,0}) = (-0.73543367,\ 1.8087622)$ $(v_{2,\alpha},\ w_{2,\alpha}) = (-0.66521082,\ -1.4463757)$ $(v_{3,\alpha},\ w_{3,\alpha}) = (-1.4104253,\ 1.7836032)$	0 0.76081722 5.2038557×10^{-3}	$7^1, 8^1$ with PD sequence to chaos.
10	$(v_{1,0},\ w_{1,0}) = (-0.73543367,\ 1.8087622)$ $(v_{2,\alpha},\ w_{2,\alpha}) = (-0.66521082,\ -1.4463757)$ $(v_{3,\alpha},\ w_{3,\alpha}) = (-1.4439419,\ 1.7666513)$	0 0.76081722 7.5281428×10^{-3}	$7^1, 8^1$ with PD sequence to chaos, 9^1 showed p-1.
11	$(v_{1,0},\ w_{1,0}) = (-0.73543367,\ 1.8087622)$ $(v_{2,\alpha},\ w_{2,\alpha}) = (-0.66521082,\ -1.4463757)$ $(v_{3,\alpha},\ w_{3,\alpha}) = (-1.4495929,\ 1.7402246)$	0 0.76081722 1.1073665×10^{-2}	$7^1, 8^1$ with PD sequence to chaos, 9^1 showed p-1.
12	$(v_{1,0},\ w_{1,0}) = (-0.73543367,\ 1.8087622)$ $(v_{2,\alpha},\ w_{2,\alpha}) = (-0.66521082,\ -1.4463757)$ $(v_{3,\alpha},\ w_{3,\alpha}) = (-1.4473132,\ 1.7111448)$	0 0.76081722 1.4973740×10^{-2}	$7^1, 8^1$ with PD sequence to chaos, 9^1 showed p-1, 2, 4.
13	$(v_{1,0},\ w_{1,0}) = (-0.73543367,\ 1.8087622)$ $(v_{2,\alpha},\ w_{2,\alpha}) = (-0.66521082,\ -1.4463757)$ $(v_{3,\alpha},\ w_{3,\alpha}) = (-1.4426890,\ 1.6665351)$	0 0.76081722 2.0984244×10^{-2}	$7^1 - 9^1$ with PD sequence to chaos.
14	$(v_{1,0},\ w_{1,0}) = (-0.73543367,\ 1.8087622)$ $(v_{2,\alpha},\ w_{2,\alpha}) = (-0.66521082,\ -1.4463757)$ $(v_{3,\alpha},\ w_{3,\alpha}) = (-1.4367779,\ 1.6107090)$	0 0.76081722 2.8557478×10^{-2}	$7^1 - 9^1$ with PD sequence to chaos.
15	$(v_{1,0},\ w_{1,0}) = (-0.73543367,\ 1.8087622)$ $(v_{2,\alpha},\ w_{2,\alpha}) = (-0.66521082,\ -1.4463757)$ $(v_{3,\alpha},\ w_{3,\alpha}) = (-1.4223418,\ 1.4769175)$	0 0.76081722 4.6949618×10^{-2}	$7^1 - 9^1$ with PD sequence to chaos.

tions [see Table IV and Figs. 14(d)–14(f)] for h in the range $1.884 \leqslant h \leqslant 2.019$. The PD and period-adding bifurcations occur as h decreases, as shown in Fig. 14(f).

The orbit diagrams in Figs. 14(g)–14(i) (see Table IV) show the results of varying a. The system shows MMOs in the range $2.9697 \leqslant a \leqslant 3.2031$ with PD MMOs (5^1–9^1) as a increases.

We studied the influence of the coupling strength on the dynamics of the system [Figs. 14(j)–14(l)]. MMOs with PD and period-adding bifurcations occur for decreasing D_w. In addition to the $9^1 - 5^1$ MMOs found on varying the other parameters, varying D_w gives extra MMOs with PD (11^1 and 10^1), as shown in Table IV and Fig. 14(l).

TABLE IX. Continuation of Table VIII.

Case	Initial conditions	Initial phase, $\phi_{i,\alpha} = \frac{t}{T}$	MMOs in Region IV
16	$(v_{1,0},\ w_{1,0}) = (-0.73543367,\ 1.8087622)$ $(v_{2,\alpha},\ w_{2,\alpha}) = (-0.66521082,\ -1.4463757)$ $(v_{3,\alpha},\ w_{3,\alpha}) = (-1.4078884,\ 1.3465270)$	0 0.76081722 6.5220803×10^{-2}	$7^1, 8^1$ with PD sequence to chaos, 9^1 showed p-1, 2.
17	$(v_{1,0},\ w_{1,0}) = (-0.73543367,\ 1.8087622)$ $(v_{2,\alpha},\ w_{2,\alpha}) = (-0.66521082,\ -1.4463757)$ $(v_{3,\alpha},\ w_{3,\alpha}) = (-1.3921840,\ 1.2088489)$	0 0.76081722 8.4910542×10^{-2}	$7^1, 8^1$ with PD sequence to chaos, No9^1.
18	$(v_{1,0},\ w_{1,0}) = (-0.73543367,\ 1.8087622)$ $(v_{2,\alpha},\ w_{2,\alpha}) = (-0.66521082,\ -1.4463757)$ $(v_{3,\alpha},\ w_{3,\alpha}) = (-1.3761427,\ 1.0724684)$	0 0.76081722 0.10484701	$7^1, 8^1$ with PD sequence to chaos, No9^1.
19	$(v_{1,0},\ w_{1,0}) = (-0.73543367,\ 1.8087622)$ $(v_{2,\alpha},\ w_{2,\alpha}) = (-0.66521082,\ -1.4463757)$ $(v_{3,\alpha},\ w_{3,\alpha}) = (-1.3608116,\ 0.94609604)$	0 0.76081722 0.12373419	7^1 with PD sequence to chaos, 8^1 had p-1, 2, 4.No9^1.
20	$(v_{1,0},\ w_{1,0}) = (-0.73543367,\ 1.8087622)$ $(v_{2,\alpha},\ w_{2,\alpha}) = (-0.66521082,\ -1.4463757)$ $(v_{3,\alpha},\ w_{3,\alpha}) = (-1.3486649,\ 0.84869818)$	0 0.76081722 0.13858228	$7^1, 9^1$ with PD sequence to chaos, 8^1 had p-1.
21	$(v_{1,0},\ w_{1,0}) = (-0.73543367,\ 1.8087622)$ $(v_{2,\alpha},\ w_{2,\alpha}) = (-0.66521082, -1.4463757)$ $(v_{3\alpha},\ w_{3,\alpha}) = (-1.3311480,\ 0.71243563)$	0 0.76081722 0.15981353	$5^1 - 7^1, 9^1$with PD sequence to chaos, 8^1 had p-1.
22	$(v_{1,0},\ w_{1,0}) = (-0.73543367,\ 1.8087622)$ $(v_{2,\alpha},\ w_{2,\alpha}) = (-0.66521082,\ -1.4463757)$ $(v_{3,\alpha},\ w_{3,\alpha}) = (-1.3109718,\ 0.56155319)$	0 0.76081722 0.18400104	$6^1, 7^1, 9^1$with PD sequence to chaos, 8^1 had p-1.
23	$(v_{1,0},\ w_{1,0}) = (-0.73543367,\ 1.8087622)$ $(v_{2,\alpha},\ w_{2,\alpha}) = (-0.66521082,\ -1.4463757)$ $(v_{3,\alpha},\ w_{3,\alpha}) = (-1.2954752,\ 0.45001601)$	0 0.76081722 0.20238354	$5^1 - 9^1$ with PD sequence to chaos.
24	$(v_{1,0},\ w_{1,0}) = (-0.73543367,\ 1.8087622)$ $(v_{2,\alpha},\ w_{2,\alpha}) = (-0.66521082, -1.4463757)$ $(v_{3,\alpha},\ w_{3,\alpha}) = (-1.2899349,\ 0.41104780)$	0 0.76081722 0.20891417	$5^1 - 9^1$ with PD sequence to chaos.
25	$(v_{1,0},\ w_{1,0}) = (-0.73543367,\ 1.8087622)$ $(v_{2,\alpha},\ w_{2,\alpha}) = (-0.66521082,\ -1.4463757)$ $(v_{3,\alpha},\ w_{3,\alpha}) = (-1.2825189,\ 0.35962892)$	0 0.76081722 0.21762167	$5^1 - 9^1$ with PD sequence to chaos.
26	$(v_{1,0},\ w_{1,0}) = (-0.73543367,\ 1.8087622)$ $(v_{2,\alpha},\ w_{2,\alpha}) = (-0.66521082,\ -1.4463757)$ $(v_{3,\alpha},\ w_{3,\alpha}) = (-1.2787984,\ 0.33415114)$	0 0.76081722 0.22197542	$5^1 - 9^1$ with PD sequence to chaos.
27	$(v_{1,0},\ w_{1,0}) = (-0.73543367,\ 1.8087622)$ $(v_{2,\alpha},\ w_{2,\alpha}) = (-0.66521082,\ -1.4463757)$ $(v_{3,\alpha},\ w_{3,\alpha}) = (-1.2713317,\ 0.28366069)$	0 0.76081722 0.23068292	$5^1 - 9^1$ with PD sequence to chaos.
28	$(v_{1,0},\ w_{1,0}) = (-0.73543367,\ 1.8087622)$ $(v_{2,\alpha},\ w_{2,\alpha}) = (-0.66521082,\ -1.4463757)$ $(v_{3,\alpha},\ w_{3,\alpha}) = (-1.2638306,\ 0.23379274)$	0 0.76081722 0.23939042	$5^1 - 9^1$ with PD sequence to chaos.
29	$(v_{1,0},\ w_{1,0}) = (-0.73543367,\ 1.8087622)$ $(v_{2,\alpha},\ w_{2,\alpha}) = (-0.66521082, -1.4463757)$ $(v_{3,\alpha}, w_{3,\alpha}) = (-1.2449229,\ 0.11186542)$	0 0.76081722 0.26115918	$5^1 - 9^1$ with PD sequence to chaos.
30	$(v_{1,0},\ w_{1,0}) = (-0.73543367,\ 1.8087622)$ $(v_{2,\alpha},\ w_{2,\alpha}) = (-0.66521082,\ -1.4463757)$ $(v_{3,\alpha}, w_{3,\alpha}) = (-1.0972651, -0.66313301)$	0 0.76081722 0.42203680	$5^1 - 9^1$ with PD sequence to chaos.

Figure 15 shows observations made for Case 1. At $\varphi = -0.69$ (Region III) all three oscillators exhibit in-phase LAOs as shown in Fig. 15(a). As φ increases in Region IV, oscillator 2 displays 5^1 MMOs [see Fig. 2(a)] while oscillators 1 and 3 exhibit out-of-phase LAOs as shown in Fig. 15(b). After the PD sequence to chaos and period-adding bifurcations, all three oscillators begin out-of-phase singly periodic oscillations as shown in Fig. 15(f). These out-of-phase singly periodic oscillations continue for a significant range of φ ($-0.648264 \leqslant \varphi \leqslant -0.582085$), after which all three oscillators transition to in-phase LAOs. Before transitioning to 6^1 MMOs, oscillator 2 shows intermittent spiking, as shown in Figs. 15(c)–15(e).

APPENDIX B: MASTER-SLAVE-LIKE FORCED SYSTEM

We calculated the Feigenbaum constant for some of the Cases in Table II (main text). The results for Cases 3 and 5 are shown in Tables V and VI, respectively.

TABLE X. Continuation of Table VIII.

Case	Initial conditions	Initial phase, $\phi_{i,\alpha} = \frac{t}{T}$	MMOs in Region IV
31	$(v_{1,0},\ w_{1,0}) = (-0.73543367,\ 1.8087622)$ $(v_{2,\alpha},\ w_{2,\alpha}) = (-0.66521082,\ -1.4463757)$ $(v_{3,\alpha},\ w_{3,\alpha}) = (-0.83268550,\ -1.3617089)$	0 0.76081722 0.66312506	$5^1 - 9^1$ with PD sequence to chaos.
32	$(v_{1,0},\ w_{1,0}) = (-0.73543367,\ 1.8087622)$ $(v_{2,\alpha},\ w_{2,\alpha}) = (-0.66521082,\ -1.4463757)$ $(v_{3,\alpha},\ w_{3,\alpha}) = (-0.66521082,\ -1.4463757)$	0 0.76081722 0.76081722	$5^1 - 9^1$ with PD sequence to chaos.
33	$(v_{1,0},\ w_{1,0}) = (-0.73543367,\ 1.8087622)$ $(v_{2,\alpha},\ w_{2,\alpha}) = (-0.66521082,\ -1.4463757)$ $(v_{3,\alpha},\ w_{3,\alpha}) = (0.15026501,\ -1.3754568)$	0 0.76081722 0.80544753	$6^1 - 9^1$ with PD sequence to chaos No 5^1.
34	$(v_{1,0},\ w_{1,0}) = (-0.73543367,\ 1.8087622)$ $(v_{2,\alpha},\ w_{2,\alpha}) = (-0.66521082,\ -1.4463757)$ $(v_{3,\alpha},\ w_{3,\alpha}) = (0.73704220,\ -1.3398600)$	0 0.76081722 0.80886316	$6^1 - 9^1$ with PD sequence to chaos, no 5^1.
35	$(v_{1,0},\ w_{1,0}) = (-0.73543367,\ 1.8087622)$ $(v_{2,\alpha},\ w_{2,\alpha}) = (-0.66521082,\ -1.4463757)$ $(v_{3,\alpha},\ w_{3,\alpha}) = (1.2102131,\ -1.2934938)$	0 0.76081722 0.81178353	$5^1,\ 6^1$ with PD sequence to chaos, no $7^1 - 9^1$.
36	$(v_{1,0},\ w_{1,0}) = (-0.73543367,\ 1.8087622)$ $(v_{2,\alpha},\ w_{2,\alpha}) = (-0.66521082,\ -1.4463757)$ $(v_{3,\alpha},\ w_{3,\alpha}) = (1.3839416,\ -1.1278747)$	0 0.76081722 0.82036018	$6^1 - 9^1$ with PD sequence to chaos No 5^1.
37	$(v_{1,0},\ w_{1,0}) = (-0.73543367,\ 1.8087622)$ $(v_{2,\alpha},\ w_{2,\alpha}) = (-0.66521082,\ -1.4463757)$ $(v_{3,\alpha},\ w_{3,\alpha}) = (1.2563883,\ -0.15799757)$	0 0.76081722 0.87135531	$6^1 - 9^1$ with PD sequence to chaos No 5^1.
38	$(v_{1,0},\ w_{1,0}) = (-0.73543367,\ 1.8087622)$ $(v_{2,\alpha},\ w_{2,\alpha}) = (-0.66521082,\ -1.4463757)$ $(v_{3,\alpha},\ w_{3,\alpha}) = (0.70889380,\ 1.6188803)$	0 0.76081722 0.97957075	$7^1 - 9^1$ with PD sequence to chaos No 5^1.6^1 had p-2.
39	$(v_{1,0},\ w_{1,0}) = (-0.73543367,\ 1.8087622)$ $(v_{2,\alpha},\ w_{2,\alpha}) = (-0.66521082,\ -1.4463757)$ $(v_{3,\alpha},\ w_{3,\alpha}) = (-0.50940690,\ 1.8157851)$	0 0.76081722 0.99930355	$8^1, 9^1$ with PD sequence to chaos. 7^1 had p-1, 2.
40	$(v_{1,0},\ w_{1,0}) = (-0.73543367,\ 1.8087622)$ $(v_{2,\alpha},\ w_{2,\alpha}) = (-0.66521082,\ -1.4463757)$ $(v_{3,\alpha},\ w_{3,\alpha}) = (-0.73543367,\ 1.8087622)$	0 0.76081722 1	1^0

APPENDIX C: UNCOUPLED FORCED SYSTEM

In addition to the 5^1 MMOs with PD to chaos seen at higher φ, we obtain several MMOs where the SAOs display complex periodicity with PD to chaos. We use the term 4^{comp} for the complex SAOs after four LAOs.

The time series [see insets of Figs. 16(a)–16(b)] and phase portraits in Figs. 16(c)–16(d) show period-1 and period-2 of 4^5 MMOs with PD. At high values of φ, the oscillator displays chaos as shown in the phase portrait and next-amplitude maps in Fig. 16(e) and Fig. 16(h), respectively.

We carried out numerical simulations to study the effect of the initial location of the oscillator on the MMOs. We place the oscillator at different positions along the cubic nullcline. At all initial locations, as long as the parameters are not changed, only 5^1 MMOs with PD are seen in addition to the other complex MMOs that show PD. We did not observe period-adding bifurcations.

Because the system is invariant to interchange of oscillators 1 and 3, we need only consider the range $0 \leqslant \theta \leqslant \pi$. As θ increases beginning with $\theta = 0$, with φ used to produce Fig. 11(h), the system shows MMOs before returning to LAOs at $\theta \approx 257\pi/512$ [Fig. 17(a)]. The system exhibits four LAOs in the MMOs with PD in the SAOs as shown in Figs. 17(b) and 17(d). The complexity in the SAOs in the PD increases with increasing θ. The PD/MMOs of particular interest is the 5^1 MMO with PD. This occurs varying θ before the system transitions to LAOs as shown in Fig. 17(c). In Fig. 17(c), there are two PD/MMOs. The first corresponds to the 5^1 and the second to 15^1 PD MMOs. Between $257\pi/512 \leqslant \theta \leqslant \pi$, only LAOs are seen.

We studied the behavior of the system varying φ at four different values of θ. Table VII shows the various observations made. Case 1, represents the sine forcing presented in the main paper.

Case 2 is noteworthy, because there is no phase difference between the forcing terms, i.e., the oscillator is forced by a single sine wave. This is similar to having the outer two oscillators start with the same initial conditions for the fully coupled system as shown in Cases 6–7, Table III. Here, however, we obtained two sets of MMOs with PD, one (3^{comp} and 4^{comp}) with complex SAOs, and the others containing combinations of 5^1 and 5^2 MMOs (Table VII). It thus appears that simple sinusoidal forcing of a single autonomous oscillator with the appropriate amplitude and frequency is sufficient to generate PD-MMOs.

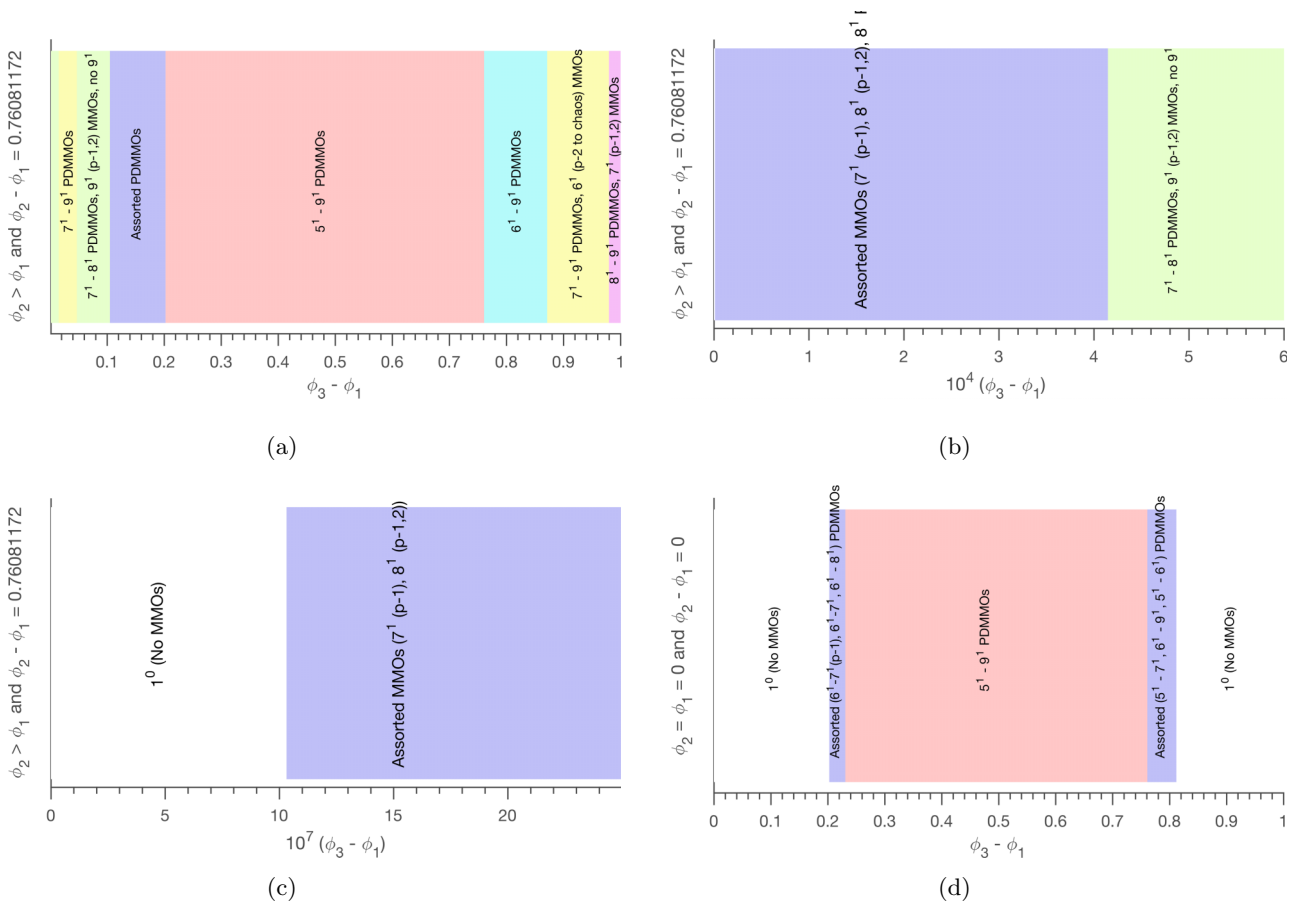

FIG. 19. 1D plot of effect of initial phase difference of oscillators with ϕ_3 varied. Parameters same as Fig. 2 initial conditions varied. (a) $\phi_2 - \phi_1$ held constant at $\phi_2 - \phi_1 \approx 0.7608$ (see Tables 19(a)–19(c)). (b) Expanded from Fig. 19(a). (c) Blowup from Fig. 19(b). (d) $\phi_2 - \phi_1$ held constant at $\phi_2 - \phi = 0$ (see Tables 19(a)–19(c)).

For Cases 3 and 4, we examined the system for changes in the observations made choosing $\theta > \pi/2$. In Case 3, we investigated the system with $\theta = 3\pi/4$. We obtained 15^1 as well as hybrid $10^1 15^1$ PD MMOs. For $\theta = \pi$ (antiphase sine forcing), the system shows only SAOs and LAOs. There are no MMOs or PD-MMOs, as shown in Case 4, Table VII.

APPENDIX D: EFFECTS OF INITIAL PHASE OF OSCILLATORS

For each set of parameters, in order to calculate the initial phase of each oscillator, we pick the point on the limit cycle of the uncoupled oscillator with the maximum value of w and call it $(v_0,\ w_0)$, defined to have phase $\phi = 0$, as shown in Fig. 18(a). All the oscillators start at a point that lies on the limit cycle of the uncoupled oscillator, Eq. (D1).

$$\begin{aligned} \frac{dv}{dt} &= -hv^3 + av - w, \\ \frac{dw}{dt} &= \varepsilon(v - \varphi). \end{aligned} \tag{D1}$$

Starting at time $t = 0$ at $(v_0,\ w_0)$, the oscillator follows the limit cycle, with its position at time t given by $[v(t),\ w(t)]$. If the period of the uncoupled limit cycle is T, then $[v(t + T),\ w(t + T)] = [v(t),\ w(t)]$. Any point $(v_\alpha,\ w_\alpha)$ picked on the limit cycle corresponds to a unique point $[v(t),\ w(t)]$ for $0 < t < T$ and its phase is calculated using Eq. (D2).

$$\phi_\alpha = \frac{t}{T}\left(\text{or } \frac{2\pi t}{T}\right). \tag{D2}$$

To assess the effects of varying the initial phases, we ran simulations with the parameters in Fig. 18. The period of the uncoupled limit cycle was determined to be $T \approx 71.55489$ as shown in Fig. 18(b). We started oscillator 1 at $\phi_{1,0} = 0$ throughout the study and varied the initial positions of oscillators 2 and 3 as $(v_{2,\alpha},\ w_{2,\alpha})$ and $(v_{3,\alpha},\ w_{3,\alpha})$, respectively. The initial phase of each oscillator, $\phi_{i,\alpha}$ (i = oscillators 1, 2 or 3) was determined from Eq. (D2).

Tables VIII–X and Figs. 19(a)–19(c) show the results obtained keeping the initial positions of oscillators 1 and 2 constant at a phase difference greater than 0.5 ($\phi_{2,\alpha} - \phi_{1,0} \approx 0.7608$). This phase difference resulted in both PD-MMOs and period-adding bifurcations (5^1–9^1). The phase difference between the outer oscillators 1 and 3 before the onset of MMOs was relatively small as shown in Case 3 ($\phi_{3,\alpha} - \phi_{1,0} \approx 2.496 \times 10^{-6}$). We observed both 7^1 and 8^1 MMOs without period-doubling sequence to chaos. As the separation between the outer oscillators increased, additional periods were added until the 8^1 MMOs showed a doubling sequence to chaos as

seen in Case 6 with $\phi_{3,\alpha} - \phi_{1,0} \approx 4.417 \times 10^{-4}$. Cases 7–22 showed MMOs both with and without PD sequence to chaos. The first appearance of all MMOs with PD is found in Case 23 with $\phi_{3,\alpha} - \phi_{1,0} \approx 0.2024$. This behavior continues for a significant range of the phase difference, until $\phi_{3,\alpha} - \phi_{1,0} \approx 0.8054$ in Case 33, where the 5^1 MMOs disappear. As the phase difference approaches 1 (Cases 33–39), the PD-MMOs slowly disappear until they vanish at $\phi_{3,\alpha} - \phi_{1,0} = 1$, Case 40.

Cases 8 and 9 of Table III demonstrate that PD-MMOs and period-adding bifurcations can occur when the initial phases of the central oscillator and one of the outer oscillators are the same. In Tables XI–XII, we set $\phi_{2,0} - \phi_{1,0} = 0$ and varied $\phi_{3,\alpha}$. Unlike Tables VIII–X where the oscillators display PD-MMOs with almost zero initial phase difference between the outer oscillators, with $\phi_{3,\alpha} - \phi_{1,0} \approx 2.496 \times 10^{-6}$, now the PD-MMOs only appear at much larger initial

TABLE XI. Oscillators 1 and 2 kept constant, $\phi_{2,alpha} - \phi_{1,0} = 0$, and varied oscillator 3.

Case	Initial conditions	Initial phase, $\phi_{i,\alpha} = \frac{t}{T}$	MMOs in Region IV
	$(v_{1,0},\ w_{1,0}) = (-0.73543367,\ 1.8087622)$	0	
1	$(v_{2,0},\ w_{2,0}) = (-0.73543367,\ 1.8087622)$	0	1^0
	$(v_{3,0},\ w_{3,0}) = (-0.73543367,\ 1.8087622)$	0	
	$(v_{1,0},\ w_{1,0}) = (-0.73543367,\ 1.8087622)$	0	
2	$(v_{2,0},\ w_{2,0}) = (-0.73543367,\ 1.8087622)$	0	1^0
	$(v_{3,\alpha},\ w_{3,\alpha}) = (-0.73567117,\ 1.8087615)$	1.0309375×10^{-6}	
	$(v_{1,0},\ w_{1,0}) = (-0.73543367,\ 1.8087622)$	0	
3	$(v_{2,0},\ w_{2,0}) = (-0.73543367,\ 1.8087622)$	0	1^0
	$(v_{3,\alpha},\ w_{3,\alpha}) = (-0.73600866,\ 1.8087606)$	2.4959578×10^{-6}	
	$(v_{1,0},\ w_{1,0}) = (-0.73543367,\ 1.8087622)$	0	
4	$(v_{2,0},\ w_{2,0}) = (-0.73543367,\ 1.8087622)$	0	1^0
	$(v_{3,\alpha},\ w_{3,\alpha}) = (-0.74095742,\ 1.8087461)$	2.3982862×10^{-5}	
	$(v_{1,0},\ w_{1,0}) = (-0.73543367,\ 1.8087622)$	0	
5	$(v_{2,0},\ w_{2,0}) = (-0.73543367,\ 1.8087622)$	0	1^0
	$(v_{3,\alpha},\ w_{3,\alpha}) = (-0.77327807,\ 1.8086264)$	1.6462444×10^{-4}	
	$(v_{1,0},\ w_{1,0}) = (-0.73543367,\ 1.8087622)$	0	
6	$(v_{2,0},\ w_{2,0}) = (-0.73543367,\ 1.8087622)$	0	1^0
	$(v_{3,\alpha},\ w_{3,\alpha}) = (-0.83020026,\ 1.8083070)$	4.1465391×10^{-4}	
	$(v_{1,0},\ w_{1,0}) = (-0.73543367,\ 1.8087622)$	0	
7	$(v_{2,0},\ w_{2,0}) = (-0.73543367,\ 1.8087622)$	0	1^0
	$(v_{3,\alpha},\ w_{3,\alpha}) = (-1.0530435,\ 1.8054960)$	1.4772792×10^{-3}	
	$(v_{1,0},\ w_{1,0}) = (-0.73543367,\ 1.8087622)$	0	
8	$(v_{2,0},\ w_{2,0}) = (-0.73543367,\ 1.8087622)$	0	1^0
	$(v_{3,\alpha},\ w_{3,\alpha}) = (-1.2996932,\ 1.7967280)$	3.2341209×10^{-3}	
	$((v_{1,0},\ w_{1,0}) = (-0.73543367,\ 1.8087622)$	0	
9	$(v_{2,0},\ w_{2,0}) = (-0.73543367,\ 1.8087622)$	0	1^0
	$(v_{3,\alpha},\ w_{3,\alpha}) = (-1.4104253,\ 1.7836032)$	5.2038557×10^{-3}	
	$(v_{1,0},\ w_{1,0}) = (-0.73543367,\ 1.8087622)$	0	
10	$(v_{2,0},\ w_{2,0}) = (-0.73543367,\ 1.8087622)$	0	1^0
	$(v_{3,\alpha},\ w_{3,\alpha}) = (-1.4439419,\ 1.7666513)$	7.5281428×10^{-3}	
	$(v_{1,0},\ w_{1,0}) = (-0.73543367,\ 1.8087622)$	0	
11	$(v_{2,0},\ w_{2,0}) = (-0.73543367,\ 1.8087622)$	0	1^0
	$(v_{3,\alpha},\ w_{3,\alpha}) = (-1.4495929,\ 1.7402246)$	1.1073665×10^{-2}	
	$(v_{1,0},\ w_{1,0}) = (-0.73543367,\ 1.8087622)$	0	
12	$(v_{2,0},\ w_{2,0}) = (-0.73543367,\ 1.8087622)$	0	1^0
	$(v_{3,\alpha},\ w_{3,\alpha}) = (-1.4473132,\ 1.7111448)$	1.4973740×10^{-2}	
	$(v_{1,0},\ w_{1,0}) = (-0.73543367,\ 1.8087622)$	0	
13	$(v_{2,0},\ w_{2,0}) = (-0.73543367,\ 1.8087622)$	0	1^0
	$(v_{3,\alpha},\ w_{3,\alpha}) = (-1.4426890,\ 1.6665351)$	2.0984244×10^{-2}	
	$(v_{1,0},\ w_{1,0}) = (-0.73543367,\ 1.8087622)$	0	
14	$(v_{2,0},\ w_{2,0}) = (-0.73543367,\ 1.8087622)$	0	1^0
	$(v_{3,\alpha},\ w_{3,\alpha}) = (-1.4367779,\ 1.6107090)$	2.8557478×10^{-2}	
	$(v_{1,0},\ w_{1,0}) = (-0.73543367,\ 1.8087622)$	0	
15	$(v_{2,0},\ w_{2,0}) = (-0.73543367,\ 1.8087622)$	0	1^0
	$(v_{3,\alpha},\ w_{3,\alpha}) = (-1.4223418,\ 1.4769175)$	4.6949618×10^{-2}	

TABLE XII. Continuation of Table XI.

Case	Initial conditions	Initial phase, $\phi_{i,\alpha} = \frac{t}{T}$	MMOs in Region IV
	$(v_{1,0},\ w_{1,0}) = (-0.73543367,\ 1.8087622)$	0	
16	$(v_{2,0},\ w_{2,0}) = (-0.73543367,\ 1.8087622)$	0	1^0
	$(v_{3,\alpha},\ w_{3,\alpha}) = (-1.4078884,\ 1.3465270)$	6.5220803×10^{-2}	
	$(v_{1,0},\ w_{1,0}) = (-0.73543367,\ 1.8087622)$	0	
17	$(v_{2,0},\ w_{2,0}) = (-0.73543367,\ 1.8087622)$	0	1^0
	$(v_{3,\alpha},\ w_{3,\alpha}) = (-1.3921840,\ 1.2088489)$	8.4910542×10^{-2}	
	$(v_{1,0},\ w_{1,0}) = (-0.73543367,\ 1.8087622)$	0	
18	$(v_{2,0},\ w_{2,0}) = (-0.73543367,\ 1.8087622)$	0	1^0
	$(v_{3,\alpha},\ w_{3,\alpha}) = (-1.3761427,\ 1.0724684)$	0.10484701	
	$(v_{1,0},\ w_{1,0}) = (-0.73543367,\ 1.8087622)$	0	
19	$(v_{2,0},\ w_{2,0}) = (-0.73543367,\ 1.8087622)$	0	1^0
	$(v_{3,\alpha},\ w_{3,\alpha}) = (-1.3608116,\ 0.94609604)$	0.12373419	
	$(v_{1,0},\ w_{1,0}) = (-0.73543367,\ 1.8087622)$	0	
20	$(v_{2,0},\ w_{2,0}) = (-0.73543367,\ 1.8087622)$	0	1^0
	$(v_{3,\alpha},\ w_{3,\alpha}) = (-1.3486649,\ 0.84869818)$	0.13858228	
	$(v_{1,0},\ w_{1,0}) = (-0.73543367,\ 1.8087622)$	0	
21	$(v_{2,0},\ w_{2,0}) = (-0.73543367,\ 1.8087622)$	0	1^0
	$(v_{3,\alpha},\ w_{3,\alpha}) = (-1.3311480,\ 0.71243563)$	0.15981353	
	$(v_{1,0},\ w_{1,0}) = (-0.73543367,\ 1.8087622)$	0	
22	$(v_{2,0},\ w_{2,0}) = (-0.73543367,\ 1.8087622)$	0	1^0
	$(v_{3,\alpha},\ w_{3,\alpha}) = (-1.3109718,\ 0.56155319)$	0.18400104	
	$(v_{1,0},\ w_{1,0}) = (-0.73543367,\ 1.8087622)$	0	
23	$(v_{2,0},\ w_{2,0}) = (-0.73543367,\ 1.8087622)$	0	1^0
	$(v_{3,\alpha},\ w_{3,\alpha}) = (-1.2954752,\ 0.45001601)$	0.20238354	
	$(v_{1,0},\ w_{1,0}) = (-0.73543367,\ 1.8087622)$	0	6^1 with PD
24	$(v_{2,0},\ w_{2,0}) = (-0.73543367,\ 1.8087622)$	0	sequence to chaos,
	$(v_{3,\alpha},\ w_{3,\alpha}) = (-1.2899349,\ 0.41104780)$	0.20891417	$7^1 p$-1.
	$(v_{1,0},\ w_{1,0}) = (-0.73543367,\ 1.8087622)$	0	$6^1,\ 7^1$ with PD
25	$(v_{2,0},\ w_{2,0}) = (-0.73543367,\ 1.8087622)$	0	sequence to chaos,
	$(v_{3,\alpha},\ w_{3,\alpha}) = (-1.2825189,\ 0.35962892)$	0.21762167	$8^1 p$-1.
	$(v_{1,0},\ w_{1,0}) = (-0.73543367,\ 1.8087622)$	0	$6^1 - 8^1$ with PD
26	$(v_{2,0},\ w_{2,0}) = (-0.73543367,\ 1.8087622)$	0	sequence to chaos,
	$(v_{3,\alpha},\ w_{3,\alpha}) = (-1.2787984,\ 0.33415114)$	0.22197542	no 5^1 and 9^1.
	$(v_{1,0},\ w_{1,0}) = (-0.73543367,\ 1.8087622)$	0	$6^1 - 8^1$ with PD
27	$(v_{2,0},\ w_{2,0}) = (-0.73543367,\ 1.8087622)$	0	sequence to chaos,
	$(v_{3,\alpha},\ w_{3,\alpha}) = (-1.2713317,\ 0.28366069)$	0.23068292	no $5^1, 9^1 p$-1, 2.
	$(v_{1,0},\ w_{1,0}) = (-0.73543367,\ 1.8087622)$	0	$5^1 - 9^1$ with PD
28	$(v_{2,0},\ w_{2,0}) = (-0.73543367,\ 1.8087622)$	0	sequence to chaos.
	$(v_{3,\alpha},\ w_{3,\alpha}) = (-1.2638306,\ 0.23379274)$	0.23939042	
	$(v_{1,0},\ w_{1,0}) = (-0.73543367,\ 1.8087622)$	0	$5^1 - 9^1$ with PD
29	$(v_{2,0},\ w_{2,0}) = (-0.73543367,\ 1.8087622)$	0	sequence to chaos.
	$(v_{3,\alpha},\ w_{3,\alpha}) = (-1.2449229,\ 0.11186542)$	0.26115918	
	$(v_{1,0},\ w_{1,0}) = (-0.73543367,\ 1.8087622)$	0	$5^1 - 9^1$ with PD
30	$(v_{2,0},\ w_{2,0}) = (-0.73543367,\ 1.8087622)$	0	sequence to chaos.
	$(v_{3,\alpha},\ w_{3,\alpha}) = (-1.0972651,\ -0.66313301)$	0.42203680	

phase differences, as shown in Table XII and Fig. 19(d), Case 24 with $\phi_{3,\alpha} - \phi_{1,0} = \phi_{3,\alpha} - \phi_{2,0} \approx 0.2089$. The phase differences between oscillators 1 and 3 are the same for Tables VIII–X and Tables XI–XIII, with the only difference being the phase difference between the outer oscillators and the central oscillator.

We carried out a third study where we kept the initial phase difference between the two outer oscillators constant and varied $\phi_{2,0}$. With $\phi_{3,\alpha} - \phi_{1,\alpha} \approx 0.7608$ all PD-MMOs (5^1–9^1) and period-adding bifurcations appear at $\phi_{2,\alpha} - \phi_{1,\alpha} \approx 0$ for all cases considered. The large initial phase difference between the outer oscillators ensures that changing the initial

TABLE XIII. Continuation of Table XI.

Case	Initial conditions	Initial phase, $\phi_{i,\alpha} = \frac{t}{T}$	MMOs in Region IV
31	$(v_{1,0},\ w_{1,0}) = (-0.73543367,\ 1.8087622)$ $(v_{2,0},\ w_{2,0}) = (-0.73543367,\ 1.8087622)$ $(v_{3,\alpha},\ w_{3,\alpha}) = (-0.83268550,\ -1.3617089)$	0 0 0.66312506	$5^1 - 9^1$ with PD sequence to chaos.
32	$(v_{1,0},\ w_{1,0}) = (-0.73543367,\ 1.8087622)$ $(v_{2,0},\ w_{2,0}) = (-0.73543367,\ 1.8087622)$ $(v_{3,\alpha},\ w_{3,\alpha}) = (-0.66521082,\ -1.4463757)$	0 0 0.76081722	$5^1 - 9^1$ with PD sequence to chaos.
33	$(v_{1,0},\ w_{1,0}) = (-0.73543367,\ 1.8087622)$ $(v_{2,0},\ w_{2,0}) = (-0.73543367,\ 1.8087622)$ $(v_{3,\alpha},\ w_{3,\alpha}) = (0.15026501,\ -1.3754568)$	0 0 0.80544753	$5^1 - 7^1$ with PD sequence to chaos, $8^1 p$-1, no 9^1.
34	$(v_{1,0},\ w_{1,0}) = (-0.73543367,\ 1.8087622)$ $(v_{2,0},\ w_{2,0}) = (-0.73543367,\ 1.8087622)$ $(v_{3,\alpha},\ w_{3,\alpha}) = (0.73704220,\ -1.3398600)$	0 0 0.80886316	$6^1 - 9^1$ with PD sequence to chaos, no 5^1.
35	$(v_{1,0},\ w_{1,0}) = (-0.73543367,\ 1.8087622)$ $(v_{2,0},\ w_{2,0}) = (-0.73543367,\ 1.8087622)$ $(v_{3,\alpha},\ w_{3,\alpha}) = (1.2102131,\ -1.2934938)$	0 0 0.81178353	$5^1,\ 6^1$ with PD sequence to chaos, no $7^1 - 9^1$.
36	$(v_{1,0},\ w_{1,0}) = (-0.73543367,\ 1.8087622)$ $(v_{2,0},\ w_{2,0}) = (-0.73543367,\ 1.8087622)$ $(v_{3,\alpha},\ w_{3,\alpha}) = (1.3839416,\ -1.1278747)$	0 0 0.82036018	1^0
37	$(v_{1,0},\ w_{1,0}) = (-0.73543367,\ 1.8087622)$ $(v_{2,0},\ w_{2,0}) = (-0.73543367,\ 1.8087622)$ $(v_{3,\alpha},\ w_{3,\alpha}) = (1.2563883,\ -0.15799757)$	0 0 0.87135531	1^0
38	$(v_{1,0},\ w_{1,0}) = (-0.73543367,\ 1.8087622)$ $(v_{2,0},\ w_{2,0}) = (-0.73543367,\ 1.8087622)$ $(v_{3,\alpha},\ w_{3,\alpha}) = (0.70889380,\ 1.6188803)$	0 0 0.97957075	1^0
39	$(v_{1,0},\ w_{1,0}) = (-0.73543367,\ 1.8087622)$ $(v_{2,0},\ w_{2,0}) = (-0.73543367,\ 1.8087622)$ $(v_{3,\alpha},\ w_{3,\alpha}) = (-0.50940690,\ 1.8157851)$	0 0 0.99930355	1^0
40	$(v_{1,0},\ w_{1,0}) = (-0.73543367,\ 1.8087622)$ $(v_{2,0},\ w_{2,0}) = (-0.73543367,\ 1.8087622)$ $(v_{3,\alpha},\ w_{3,\alpha}) = (-0.73543367,\ 1.8087622)$	0 0 1	1^0

phase of oscillator 2 does not significantly influence the behavior of the system.

The above studies conducted varying the initial phase of oscillator 3 ($\phi_{3,\alpha}$) and keeping the initial phases of oscillators 1 and 2 ($\phi_{1,0},\ \phi_{2,\alpha}$) constant suggest that if the phase difference between oscillator 1 and 2 is sufficiently large, MMOs with and without PD occur over a broad range of $\phi_{3,\alpha}$, as shown in Tables VIII–X, Figs. 19(a)–19(c). However, if the initial phase difference between oscillators 1 and 2 (any of the outer and the central oscillator) is close to zero, the PD-MMOs occur over a much narrower range of $\phi_{3,\alpha}$, as shown in Tables XI–XIII, Fig. 19(d).

[1] M. Rachwalska and A. L. Kawczyński, J. Phys. Chem. A **105**, 7885 (2001).
[2] V. S. M. Piassi, A. Tufaile, and J. C. Sartorelli, Chaos **14**, 477 (2004).
[3] A. Granados, L. Alsedà, and M. Krupa, SIAM Rev. **59**, 225 (2017).
[4] T. Kousaka, Y. Ogura, K. Shimizu, H. Asahara, and N. Inaba, Physica D **353–354**, 48 (2017).
[5] J. L. Hudson, M. Hart, and D. Marinko, J. Chem. Phys. **71**, 1601 (1979).
[6] M. Orban and I. R. Epstein, J. Phys. Chem. **86**, 3907 (1982).
[7] J. Maselko and H. L. Swinney, J. Chem. Phys. **85**, 6430 (1986).
[8] K. Showalter, R. M. Noyes, and K. Bar-Eli, J. Chem. Phys. **69**, 2514 (1978).
[9] L. Györgyi and R. J. Field, Nature (London) **355**, 808 (1992).
[10] V. Petrov, S. K. Scott, and K. Showalter, J. Chem. Phys. **97**, 6191 (1992).
[11] V. A. Makarov, V. I. Nekorkin, and M. G. Velarde, Phys. Rev. Lett. **86**, 3431 (2001).
[12] A. Alonso and R. R. Llinás, Nature (London) **342**, 175 (1989).
[13] C. A. D. Negro, C. G. Wilson, R. J. Butera, H. Rigatto, and J. C. Smith, Biophys. J. **82**, 206 (2002).
[14] J. Drover, J. Rubin, J. Su, and B. Ermentrout, SIAM J. Appl. Math. **65**, 69 (2004).
[15] G. S. Medvedev and J. E. Cisternas, Physica D **194**, 333 (2004).
[16] I. Erchova and D. J. McGonigle, Chaos **18**, 015115 (2008).

[17] C. Iglesias, C. Meunier, M. Manuel, Y. Timofeeva, N. Delestrée, and D. Zytnicki, J. Neurosci. **31**, 5829 (2011).
[18] B. J. Bacak, T. Kim, J. C. Smith, J. E. Rubin, and I. A. Rybak, eLife **5**, e13403 (2016).
[19] B. V-Ghaffari, M. Kouhnavard, and S. M. Elbasiouny, PLoS One **12**, e0178244 (2017).
[20] F. N. Albahadily, J. Ringland, and M. Schell, J. Chem. Phys. **90**, 813 (1989).
[21] M. Schell and F. N. Albahadily, J. Chem. Phys. **90**, 822 (1989).
[22] F. Plenge, P. Rodin, E. Schöll, and K. Krischer, Phys. Rev. E **64**, 056229 (2001).
[23] M. T. Koper, Physica D **80**, 72 (1995).
[24] N. Baba and K. Krischer, Chaos **18**, 015103 (2008).
[25] K. Shimizu, Y. Saito, M. Sekikawa, and N. Inaba, Physica D **241**, 1518 (2012).
[26] R. Iosub, D. Avitabile, L. Grant, K. Tsaneva-Atanasova, and H. J. Kennedy, Biophys. J. **108**, 1003 (2015).
[27] H. Baldemir, D. Avitabile, and K. Tsaneva-Atanasova, Communications in Nonlinear Science and Numerical Simulation **80**, 104979 (2020).
[28] F. Dumortier and R. Roussarie, in *Multiple-Time-Scale Dynamical Systems*, edited by C. K. R. T. Jones and A. I. Khibnik (Springer, New York, 2001), pp. 29–63.
[29] H. Rotstein, N. Kopell, A. Zhabotinsky, and I. Epstein, SIAM J. Appl. Math. **63**, 1998 (2003).
[30] G. C. Kember, G. A. Fenton, J. A. Armour, and N. Kalyaniwalla, Phys. Rev. E **63**, 041911 (2001).
[31] W. E. Sherwood, Fitzhugh–nagumo model, in *Encyclopedia of Computational Neuroscience*, edited by D. Jaeger and R. Jung (Springer, New York, 2013), pp. 1–11.
[32] N. M. Awal, D. Bullara, and I. R. Epstein, Chaos **29**, 013131 (2019).
[33] N. M. Awal and I. R. Epstein, Phys. Rev. E **101**, 042222 (2020).
[34] J. Xie, H.-C. Kao, and E. Knobloch, Phys. Rev. E **91**, 032918 (2015).
[35] C. R. Laing, Physica D **238**, 1569 (2009).
[36] C.-U. Choe, R.-S. Kim, and J.-S. Ri, Phys. Rev. E **96**, 032224 (2017).
[37] See Supplemental Material at http://link.aps.org/supplemental/10.1103/PhysRevE.104.024211 for supplemental videos.
[38] A. Wolf, J. B. Swift, H. L. Swinney, and J. A. Vastano, Physica D **16**, 285 (1985).
[39] N. Metropolis, M. Stein, and P. Stein, J. Comb. Theory, Ser. A **15**, 25 (1973).
[40] S. H. Strogatz, *Nonlinear Dynamics and Chaos: With Applications to Physics, Biology, Chemistry and Engineering* (Westview Press, Milton Park, 2000).
[41] M. J. Feigenbaum, Universality in complex discrete system, Los Alamos Theoretical Division Annual Report 1975–1976, 1976.
[42] N. Inaba and T. Kousaka, Physica D **401**, 132152 (2020).
[43] E. Kutafina, Comp. Appl. Math. **34**, 81 (2015).